RESEARCH REPORT
RESULTS OF TEST ON A MODIFIED FRACTURING/CEMENTING TRAILER FRAME

by

Bret Turley
and
Benjamin J. Wallace
and
Thomas M. Murray

Submitted to

Halliburton Services
Duncan, Oklahoma

Report No. FSEL/HALLIBURTON 86-01

November 1986

FEARS STRUCTURAL ENGINEERING LABORATORY
School of Civil Engineering and Environmental Science
University of Oklahoma
Norman, Oklahoma 73019

TABLE OF CONTENTS

Page

LIST OF FIGURES. ii

LIST OF TABLES iii

Chapter

I. INTRODUCTION 1

1.1 Objective 1
1.2 Scope 1

II. TEST DETAILS 4

2.1 Test Specimen 4
2.2 Test Setup. 6
2.3 Instrumentation 8
2.4 Testing Procedures. 12

III. TEST RESULTS 19

3.1 Brittle Lacquer Analysis Results. 19
3.2 Static Test Results 20
3.3 Fatigue Test Results. 21

IV. SUMMARY. 26

APPENDIX A - SPECIMEN DIMENSIONS, PROPERTIES, AND ANALYSIS RESULTS. A.1

APPENDIX B - STATIC TEST RESULTS B.1

LIST OF FIGURES

Figure		Page
1.1	Test Specimen and Whiffletree.	2
2.2	Locations of Measured Sections	5
2.3	Location of Cracked Welds.	7
2.4	Repair of Cracked Welds.	7
2.5	Whiffletree Details.	9
2.6	Locations of Strain Gages on Inside of Beam Web. .	11
2.7	Locations of Strain Gages on Outside of Beam Web .	13
2.8	Locations of Strain Gages on Beam Flange	14
2.9	Spacing of Strain Gages on Beam Flanges	15
2.10	Region Analyzed with Brittle Laquer Coating. . . .	17
3.1	Location of Cracking (Driver's Side Beam).	22
3.2	Location of Cracking (Passenger's Side Beam) . . .	22
3.3	Cracks Located on Driver's Side Beam	25
3.4	Cracks Located on Passenger's Side Beam.	25
A.1	Dimensions Measured at Each Cross Section.	A.1

LIST OF TABLES

Table		Page
4.1	Maximum Uniaxial Stress.	31
4.2	Maximum Von Mises Stress	32
A.1	Cross Section Dimensions	A.2
A.2	Cross Section Properties	A.3
A.3	Stiffness Analysis Results	A.4

CHAPTER 1

INTRODUCTION

1.1 Objective

This report documents the results of the third and final phase of a series of tests conducted at the Fears Structural Engineering Laboratory (FSEL) of the University of Oklahoma on a pair of built-up curved beams. These beams are used as frame rails by Halliburton Services Inc. in the manufacture of cementing and fracturing equipment trailers. The purpose of this research project was to evaluate the behavior of a modified design of the beams.

1.2 Scope

A single modified trailer frame consisting of two curved beams and the associated crossmembers was tested in this study. This frame was supported at each end by stands resting on the laboratory reaction floor. A whiffletree was used to distribute the total force to each of the two beams at two points as shown in Figure 1.1.

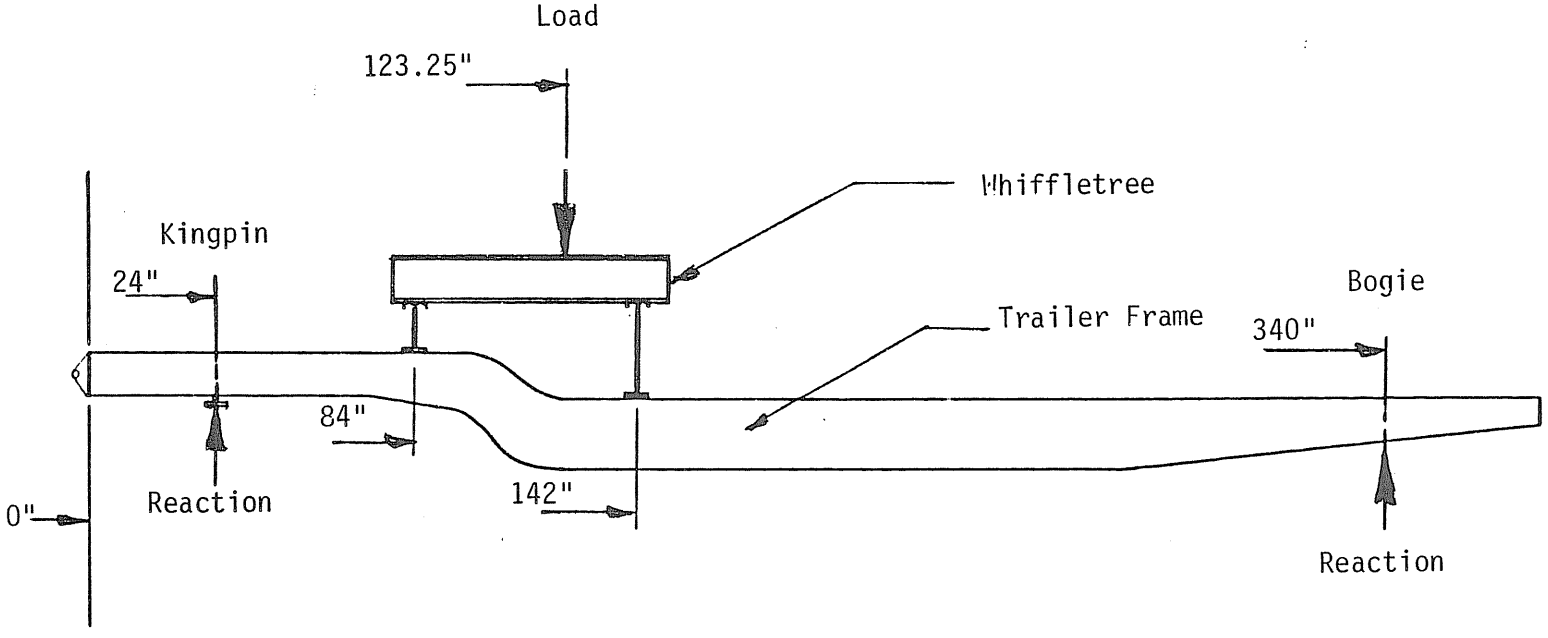

Figure 1.1 Test Specimen and Whiffletree

Experimentation on the curved beams included a brittle lacquer analysis, static tests, and fatigue tests. The brittle lacquer analysis was conducted to locate the most highly stressed regions in the curved portion of one beam. Data was collected during the static test to determine load-deflection and load-strain relationships for the beams. The fatigue test was conducted to determine the fatigue life of the beams under the idealized load used.

In addition to the experimentation conducted on the curved beams, various sections of the frame were measured, the resulting section properties calculated, and a stiffness analysis performed using these properties. This analysis was conducted to obtain a theoretical load-deflection relationship to compare with the experimentally determined value.

CHAPTER II

TEST DETAILS

2.1 Test Specimen

The test specimen was a modified trailer frame manufactured by Halliburton Services Inc. specifically for this test program. This frame consisted of the two curved beams under study which were the side rails, and connecting crossmembers. Overall dimensions of the beams are shown in Fig. 2.1. Measurements of the passenger's side beam web and flanges were made at the sections shown in Fig. 2.2. The parameters measured are shown in Fig. A.1 and listed in Table A.1 of Appendix A. Properties of the cross sections were calculated and are listed in Table A.2 of Appendix A.

The specimen was manufactured from Nicop-80, which is a high strength, low alloy steel meeting the requirements of ASTM A710-79 Type A. This material has specified yield and tensile strengths of 75 and 85 ksi in the thicknesses used.

Prior to testing, cracks were discovered by laboratory personnel in the welds splicing the top flanges of the

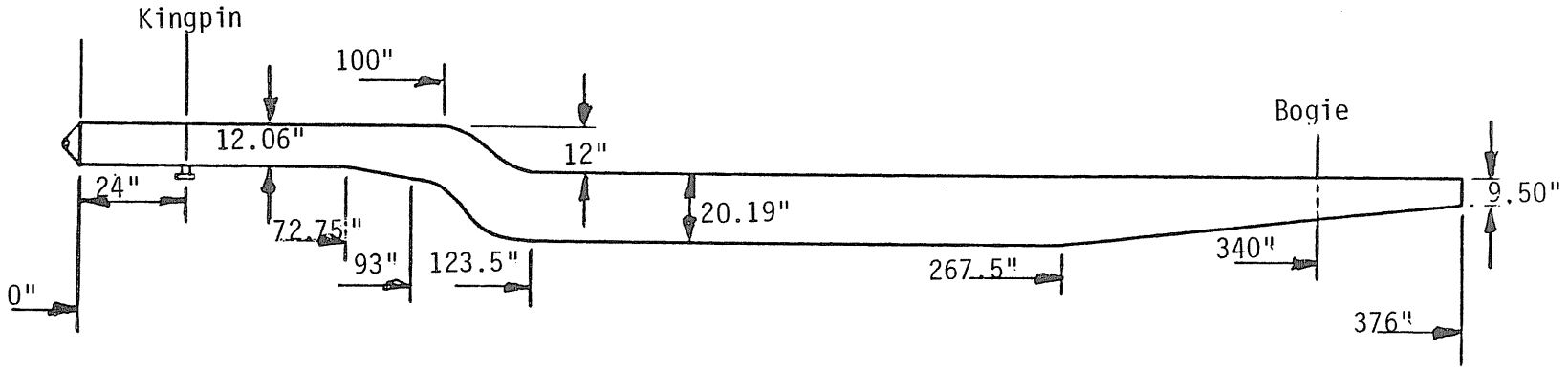

Figure 2.1 Specimen Dimensions

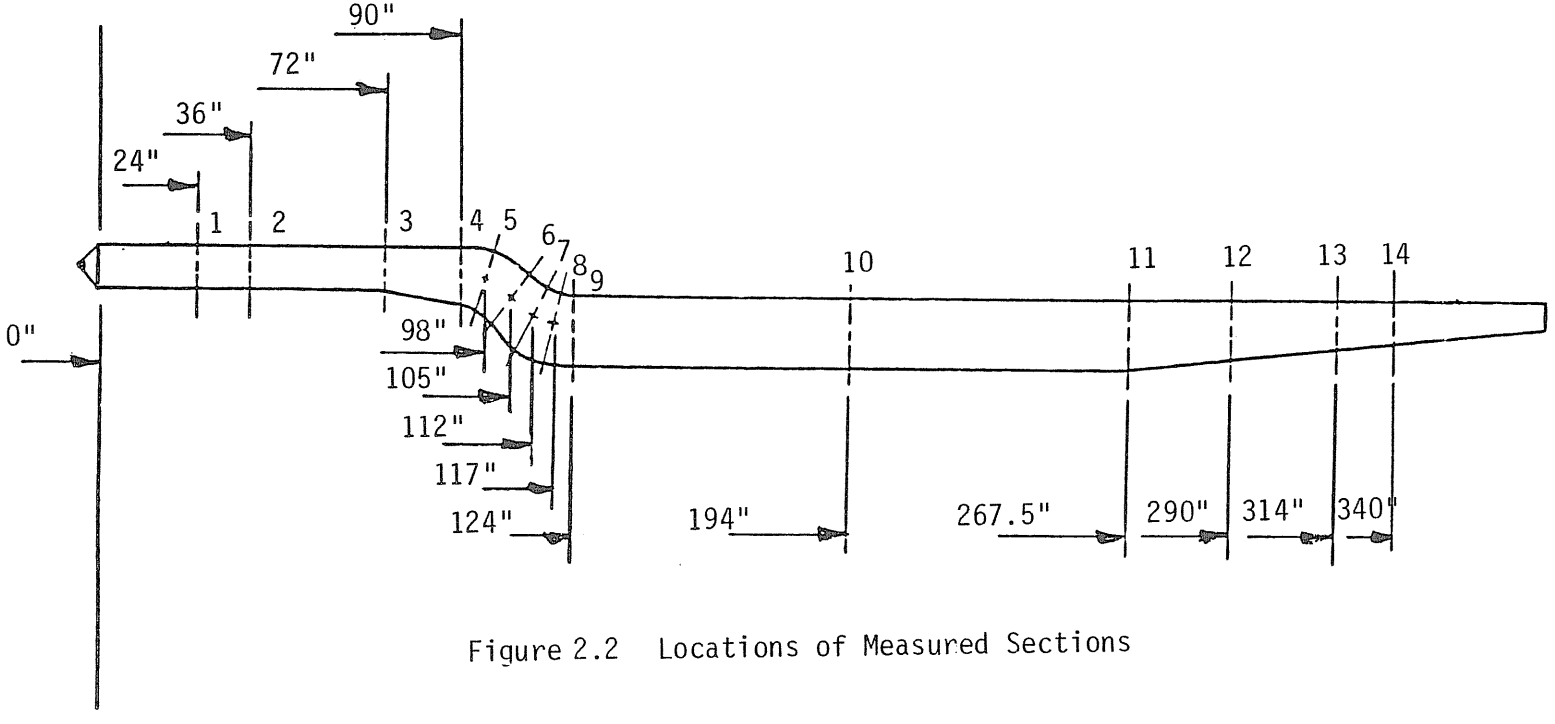

Figure 2.2 Locations of Measured Sections

curved section to the top flanges of the straight beam section. This location corresponds to section 9 of Figure 2.2 and is located 124 inches from the front of the trailer frame. Fig. 2.3 shows one of these cracks. Halliburton personnel were sent to inspect and repair the cracked welds. Upon examination, it was deemed necessary that the welds joining the formed top flanges to the web of the curved beam portion of both beams also be repaired. All defective welds were subsequently gouged out, ground smooth, and new weld material deposited. Fig. 2.4 shows the repair operation in progress. The repair was successful as none of these welds failed during the testing program.

2.2 Test Setup

The front of the specimen was supported by a fifth wheel mounted on a stand which rested on the static reaction floor of Fears Lab. The fifth wheel included a hinge which allowed the trailer frame to rock, resulting in zero moment at the kingpin location. The rear of each beam was supported at the trailer bogie centerline by an elastomeric bearing pad and a steel stand which rested on the reaction floor as shown in Figure 1.1. The elastomeric pad in each of these rear supports allowed the trailer frame to rock with no moment at the support.

A whiffletree was used to distribute the applied load

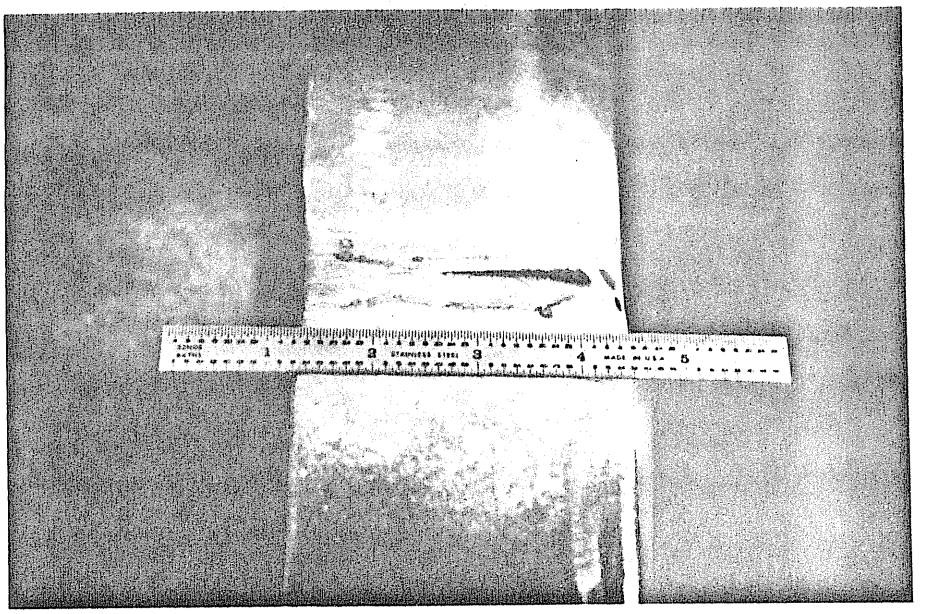

Figure 2.3 Location of Cracked Welds

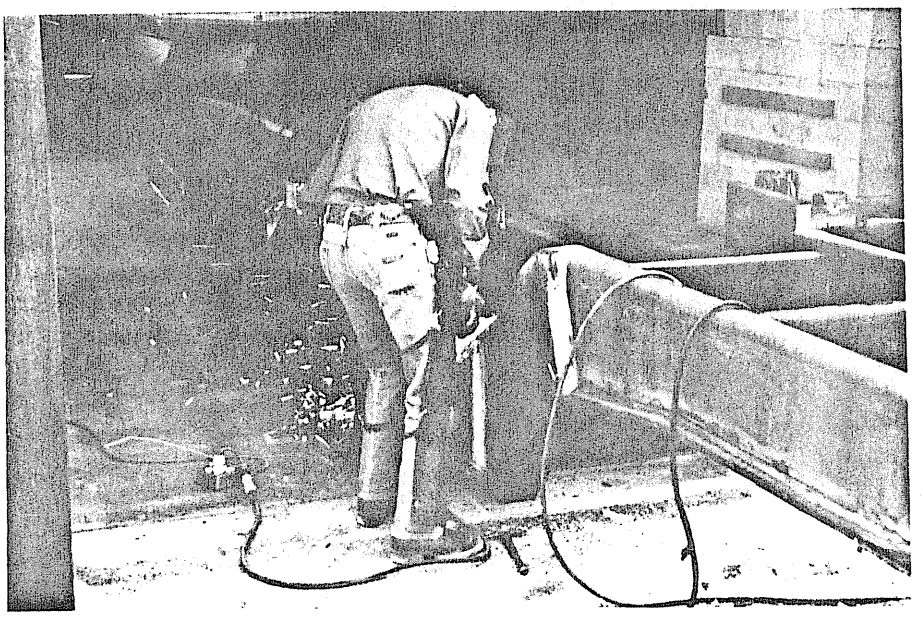

Figure 2.4 Repair of Cracked Welds

to two points on each of the two curved beams. The whiffletree, shown in Fig. 2.5, consisted of one longitudinal and two cross beams. The longitudinal beam distributed the actuator load to the cross beams in proportions calculated to produce a moment diagram in the curved beams which was similar to that produced by normal service loading. Moment diagrams supplied by Halliburton for rails of a fracturing unit and the passenger's side rail of a cementing unit were considered to be normal service loading. The whiffletree cross beams distributed their portion of the total load equally between the two curved beams.

Load was applied with a 55 kip capacity MTS actuator connected to the whiffletree. The other end of the actuator was connected to a reaction frame which spanned the specimen and was bolted to the reaction floor. The actuator was controlled with an MTS 406 controller and 436 control unit which included a cycle counter and function generator. Hydraulic power was provided by an MTS 10 gpm pumping unit.

2.3 Instrumentation

Different quantities were measured during the various tests conducted on the specimen. Total load applied was measured in all tests. Vertical deflections of each curved beam were measured during all static tests.

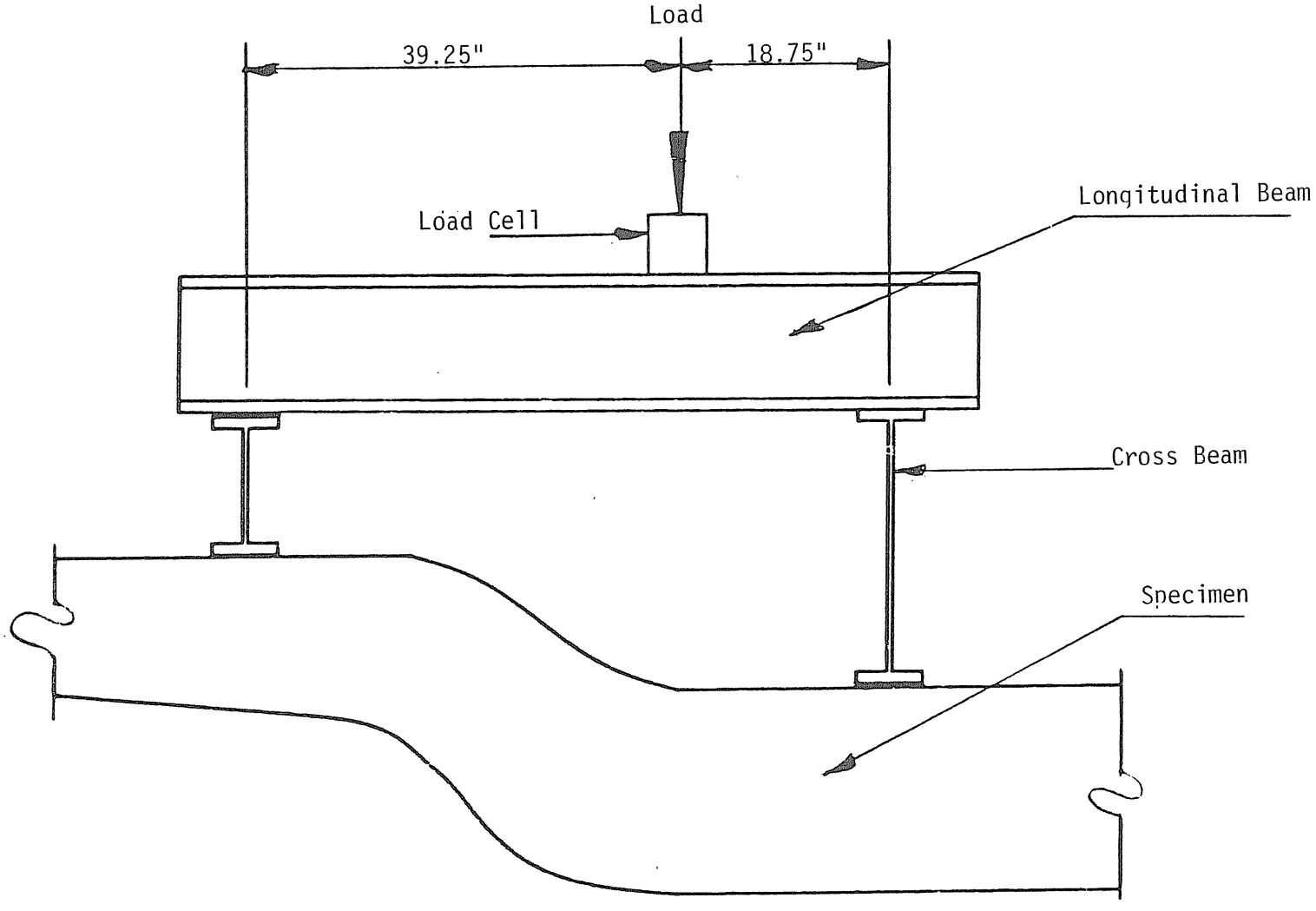

Figure 2.5 Whiffletree Details

Measurements collected during the static tests were taken with a Hewlett-Packard 3497A Data Acquisition and Control Unit driven by an IBM PC-XT microcomputer. All data was plotted on a H-P 7475A X-Y plotter driven by an IBM PC microcomputer.

Total load applied by the actuator was measured by an electronic load cell mounted on the whiffletree as shown in Fig. 2.5. The MTS control console provided excitation, signal conditioning, and a display for this transducer.

Wire potentiometers were used to measure the vertical displacement of each curved beam just behind the curved portion as shown in Fig. 2.6. These transducers were held to the reaction floor with weights and the wire was attached to the lower flange near the beam web with small magnets. These transducers were excited with a 5 volt power supply and the resulting signal was read directly with the H-P data acquisition systems during the static tests.

Electrical resistance strain gages were applied to the web and both upper and lower flanges in the curved region of the passenger's side beam. First, an area of mill scale was removed from the steel surface with an abrasive flap wheel. Next, a conditioner fluid was applied to the area and then wiped with a neutralizer solution. After this surface preparation, the gages were glued to the specimen with

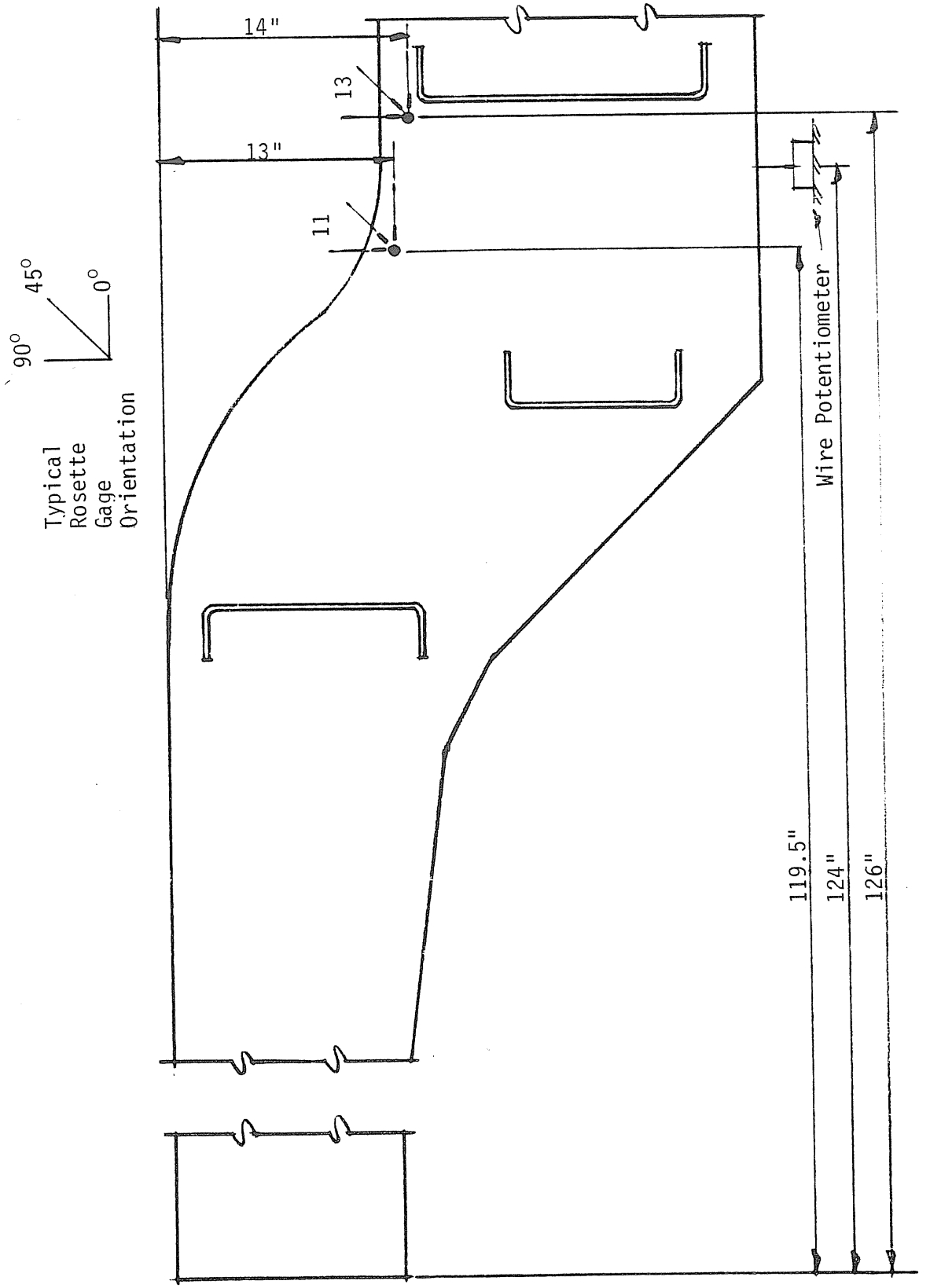

Figure 2.6 Location of Strain Gages on Inside of Beam Web

cyanoacrylic adhesive. A total of nine 0-45-90° rosette gages were applied to the beam web. Locations and orientations of these gages are shown in Figs. 2.6 and 2.7. A total of thirteen uniaxial strain gages were installed on the top and bottom surfaces of the upper and lower flanges, respectively. These gages were oriented with their active axes parallel to the beam flange and installed at the locations indicated in Fig. 2.8. Locations of these gages were specified by Halliburton personnel. The spacing of the uniaxial strain gages located on the bottom side of the lower beam flange and top side of the upper beam flange are shown in Figs. 2.9(a) and 2.9(b), respectively.

2.4 Testing Procedures

Three types of testing procedures were conducted on the specimen in this program. A brittle lacquer analysis was conducted to indicate the most highly strained regions in the curved portion of the beams. Static tests were then used to measure and record strains and deflections at specific locations under various loads. This data was collected for comparison with analytical studies and predictions of fatigue life based on maximum stresses. Fatigue testing was conducted to determine the number of loading cycles the frame could withstand before cracks could be detected.

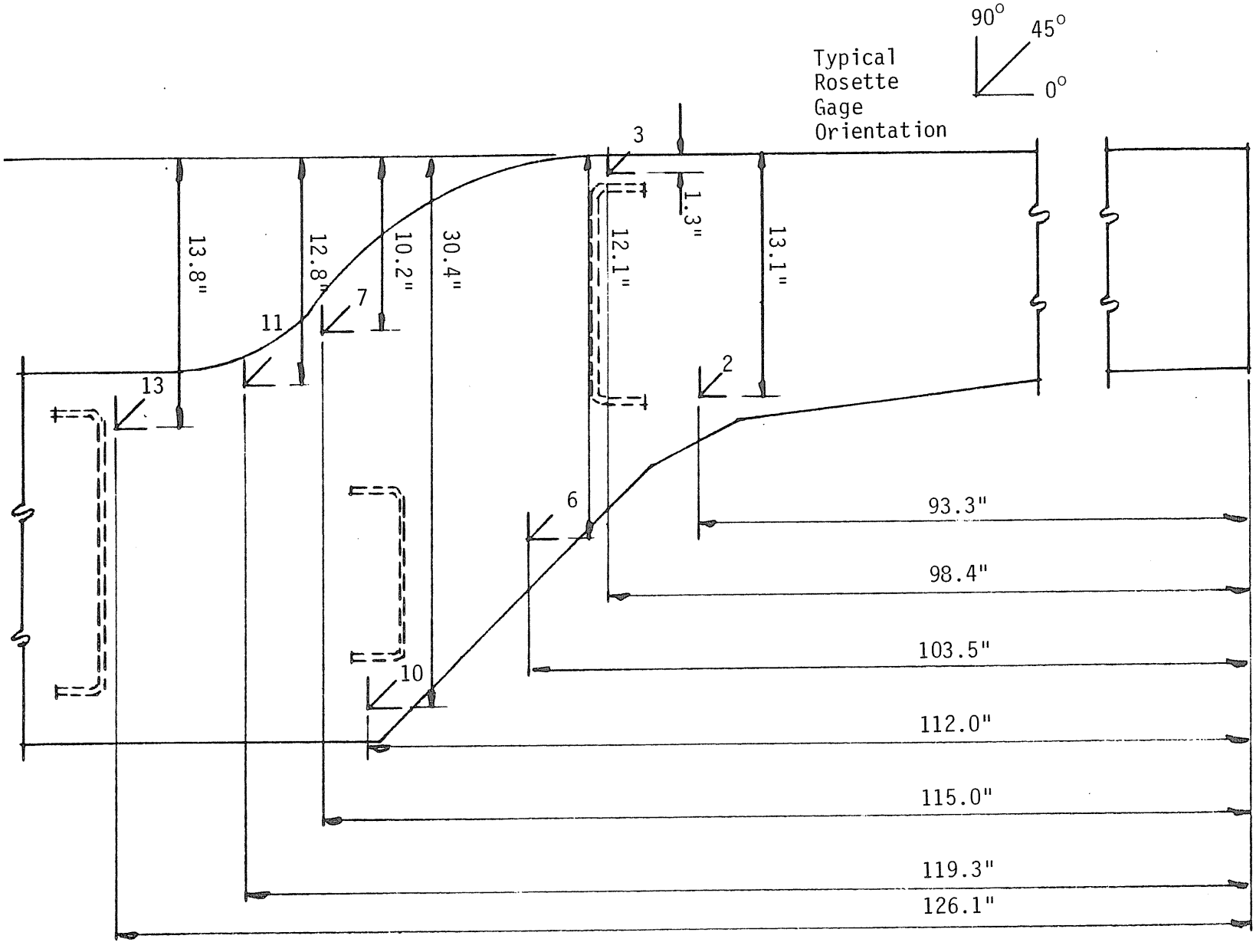

Figure 2.7 Location of Strain Gages on Outside of Beam Web

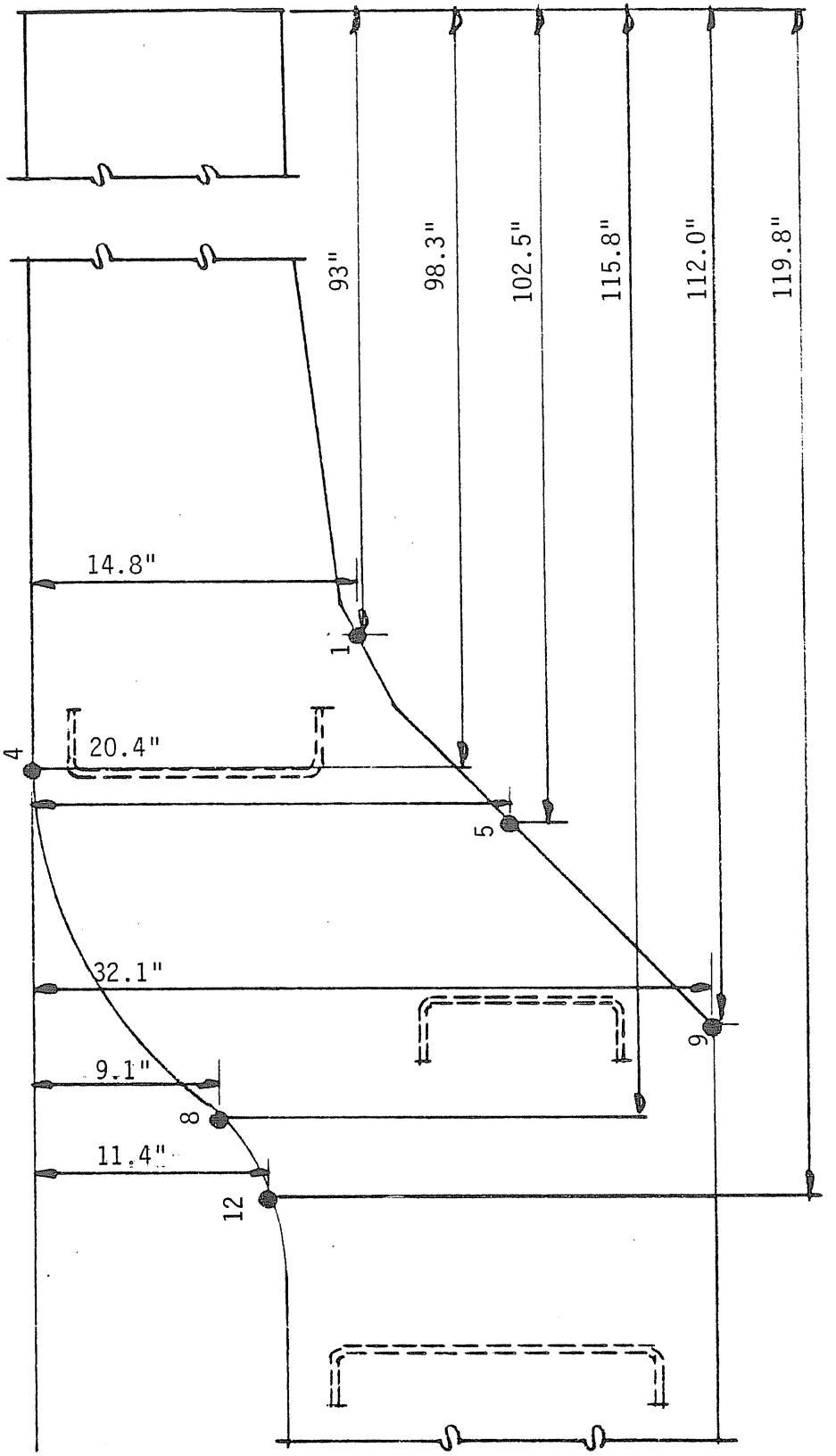

Figure 2.8 Location of Strain Gages on Beam Flange

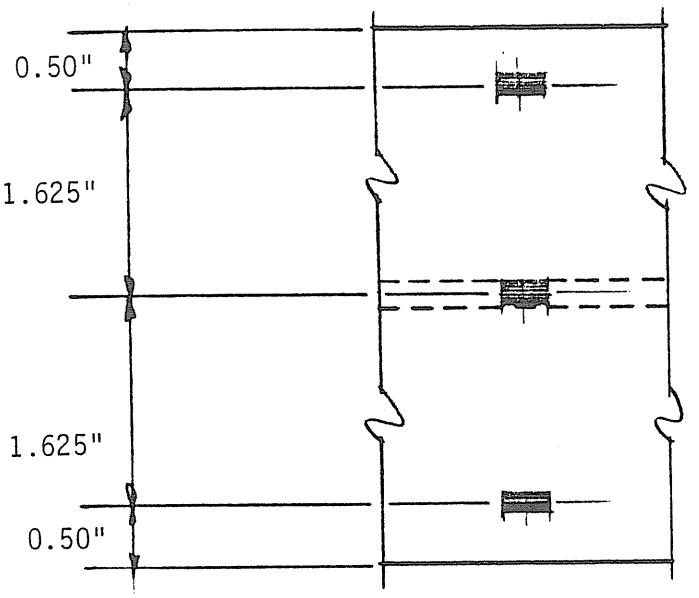

(a) Spacing of Strain Gages on Bottom of Beam Lower Flange

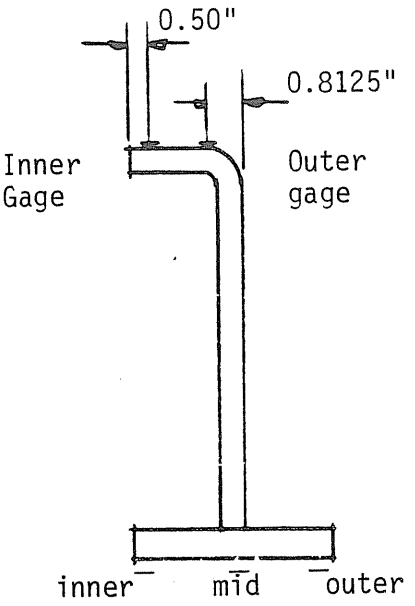

(b) Spacing of Strain Gages on Top Side of Beam Upper Flange

Figure 2.9 Spacing of Strain Gages on Beam Flanges

Brittle Lacquer Analysis

The first experimentation on the curved beams was a brittle lacquer analysis. This analysis was conducted on the lower flange and adjacent web in the curved area of the driver's side beam as shown in Fig. 2.10. This area was first wire brushed to remove mill scale. Next, the beam area and five calibration bars were coated with a reflective paint so that cracks in the lacquer could be more easily observed. Six coats of brittle lacquer were then applied to the beam and calibration bars. After allowing the lacquer to dry, the calibration bars were placed in a fixture and bent to a known deflection to determine the strain at which the lacquer first cracked. Load was then applied to the frame in 5 kip increments and the region coated with the brittle lacquer was checked for cracking.

Static Test Procedure

Static tests were used to measure deflections and strains while the load was held constant so that the 3496A could scan all the data channels at the same load and displacement. These readings were taken at various intensities of load so that load-strain and load-deflection relationships could be determined. In preparation for these tests, all available instrumentation was connected to the HP 3496A data acquisition and control unit.

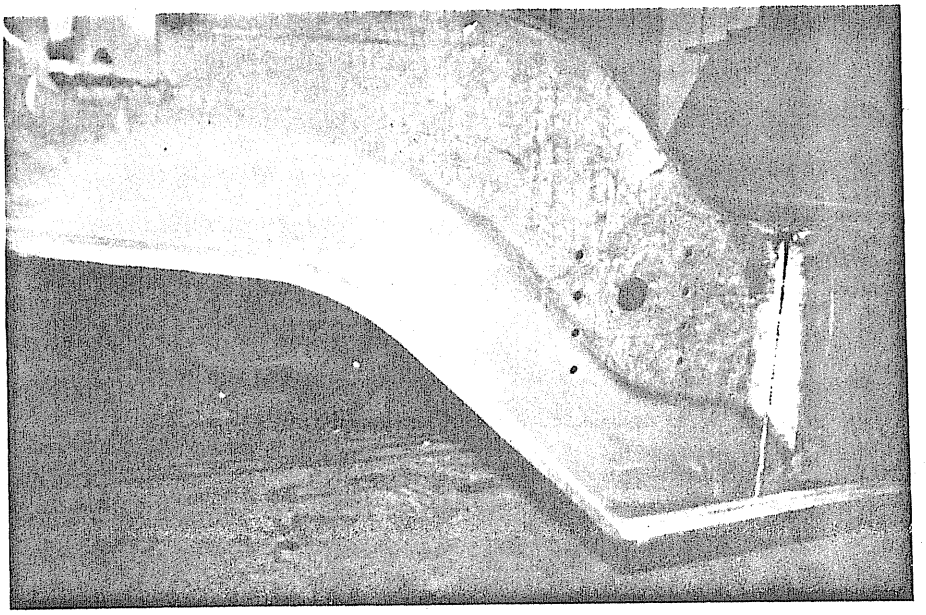

Figure 2.10 Region Analyzed with Brittle Lacquer Coating

The tests were initiated by starting the MTS system and reading all data channels while the load was zero. The load was then applied in 5 kips increments and the data channels read after each increment of load. This procedure was continued until the maximum load of 46.1 kips was reached. The specimen was then unloaded in 10 kip increments and data was collected during each unloading increment.

Fatigue Test Procedure

Fatigue testing was accomplished by programming the MTS 406 controller and 436 control unit to operate the actuator in displacement cycles which would result in the desired loads. The minimum and maximum loads reached during each cycle, 21.3 and 46.1 kips, were applied at a frequency of 1.3 Hz. These loads were chosen because they result in moments in the trailer gooseneck which are similar to those caused by one and two times the static service load, respectively.

The cyclic fatigue load was applied to the curved beams to simulate the beam flexure as the trailer is transported over a rough road. The beams were subjected to one million cycles of loading.

CHAPTER III

TEST RESULTS

This section presents results of all tests performed during this study. Results presented include those from the brittle lacquer analysis, static test, and fatigue test.

3.1 Brittle Lacquer Analysis Results

The brittle lacquer analysis was conducted to indicate the magnitude of strains present. The sensitivity of the brittle lacquer used in this test was measured with the calibration bars described in Section 2.3. By bending the five calibration bars and noting the limit of the cracked region in the coating of each bar, the lacquer sensitivity was determined to be approximately 900 x 10^{-6} inches/inch.

During the test, load was applied to the whiffletree in 5 kip increments. Between each increment of loading and the next, the coating on the specimen was inspected for cracks which would indicate areas where the strain exceeded 900 x 10^{-6} inches/inch. No cracking was observed at each of the

five kip increments to a total load of 40 kips, indicating strain less than 900 microstrain.

3.2 Static Test Results

The static test was conducted to determine load-deflection and load-strain relationships for various locations on the curved beams. Locations and directions of the measured quantities are shown in Figures 2.6 through 2.9.

This test was performed just after the specimen had been repaired. Results of this test are presented in Appendix B. Quantities measured include load, vertical deflection of each curved beam, and strain at various gages.

A stiffness analysis was performed on the trailer beams using the section properties given in Appendix A and a plane-frame program written at Fears Lab. The resulting relationship between total load and deflection is plotted along with the experimentally obtained results in Fig. B.3 of Appendix B.

3.3 Fatigue Test Results

Fatigue loading was applied to the specimen as described in Section 2.5. The counter was set to zero at the beginning of the test program and was not reset during this project. This procedure resulted in a count which represents the total number of cycles applied to the specimen since the start of the test program.

The first crack was noticed at the toe (adjacent to the beam web) of the weld joining the crossmember to the driver's side beam web as shown in Fig. 3.1. This crack was first observed at approximately 690,000 cycles. This crack initiated in the curved beam region at the radius of the crossmember where the beam web joins the crossmember upper flange and propagated along the width of the flange. This cracking was probably caused by the large out-of-plane strains due to the restraining effects of the crossmember on beam flange rolling.

The second crack was noticed at approximately 802,000 cycles at the toe (adjacent to the crossmember) of the weld where the first crack was observed. This crack initiated at the radius described previously, but propagated diagonally, along the face of the weld. In addition, the first crack was approximately 0.5 inches shorter than the

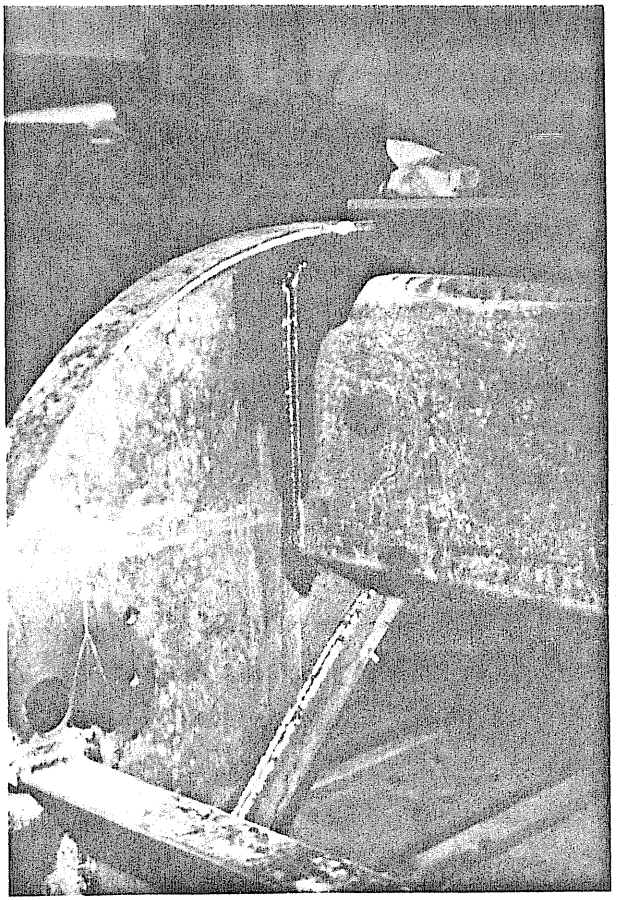

Figure 3.1 Location of Cracking (Driver's Side Beam)

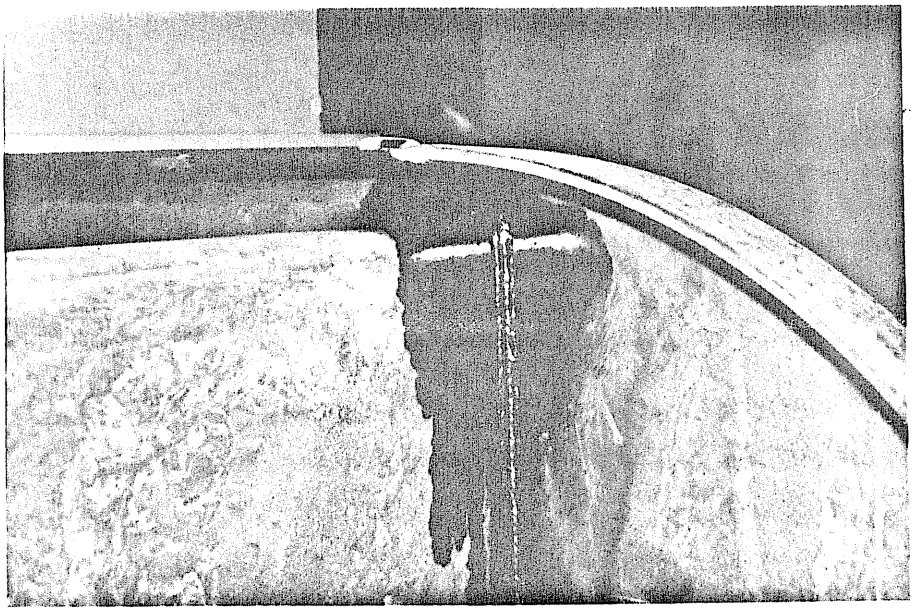

Figure 3.2 Location of Cracking (Passenger's Side Beam)

width of the crossmember flange, and the separation of the toe of the weld from the beam web was becoming easily defined without the aid of magnification.

The third crack was noticed at the toe (adjacent to the web) of the weld joining the crossmember to the passenger's side beam web. This crack was first observed at 802,000 cycles. This small crack initiated at the radius (similar to that described previously). Figure 3.2 shows the location of cracking.

The fourth crack was noticed occurring in the same proximity of the third crack at approximately 840,000 cycles. This crack initiated near the same point where the third crack initiated, but propagated diagonally away from the weld (and) into the web to a length of approximately 0.25 inches. Cracking was limited to the inside surface of the beam web only.

The fifth and sixth cracks were noticed in the driver's side beam web at approximately 930,000 cycles. The fifth crack initiated at the radius (described previously), and propagated diagonally away from the weld and into the beam web to a length of 0.5 inches but was restricted to the inside surface of the beam web only. The sixth crack initiated approximately 1 inch below the fifth crack and

propagated parallel to the same, and into the beam web to a length of approximately 0.25 inches. Cracking was restricted to the inside surface of the beam web. In addition, the first crack was equal in length to the crossmember flange width and the separation between the weld and beam web was readily visible.

The seventh crack was noticed in the inside surface of the passenger's side beam web at approximately 940,000 cycles. This crack initiated at the toe (adjacent to the beam web) of the weld joining the crossmember to the passenger's side beam web approximately 0.25 inches below the third crack and propagated parallel to the same into the beam web to a length of 0.25 inches.

Fatigue testing was terminated at a count of 1,000,000 cycles, which was the criteria defined for this test. A cleaning solution was applied to the cracked areas and wiped clean. Next, a dye penetrant was applied for five minutes to be absorbed into the cracks. The excess dye penetrant was wiped away and a developer was applied. The specimen was then loaded to 46.1 kips (twice the service load), and a photographic record was made. Figures 3.3 and 3.4 show the cracks on the driver's side and passenger's side beam, respectively.

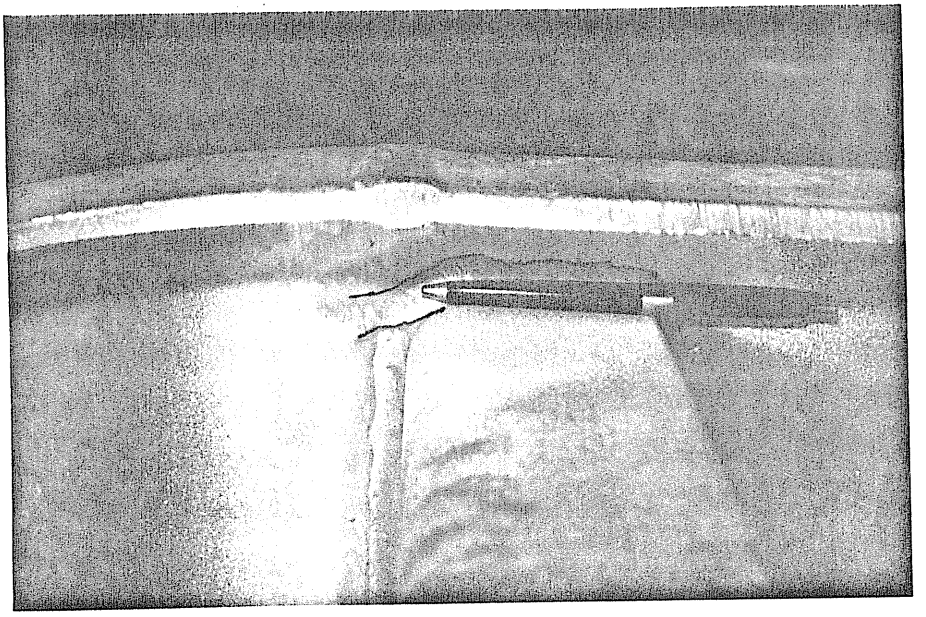

Figure 3.3 Cracks Located on Driver's Side Beam

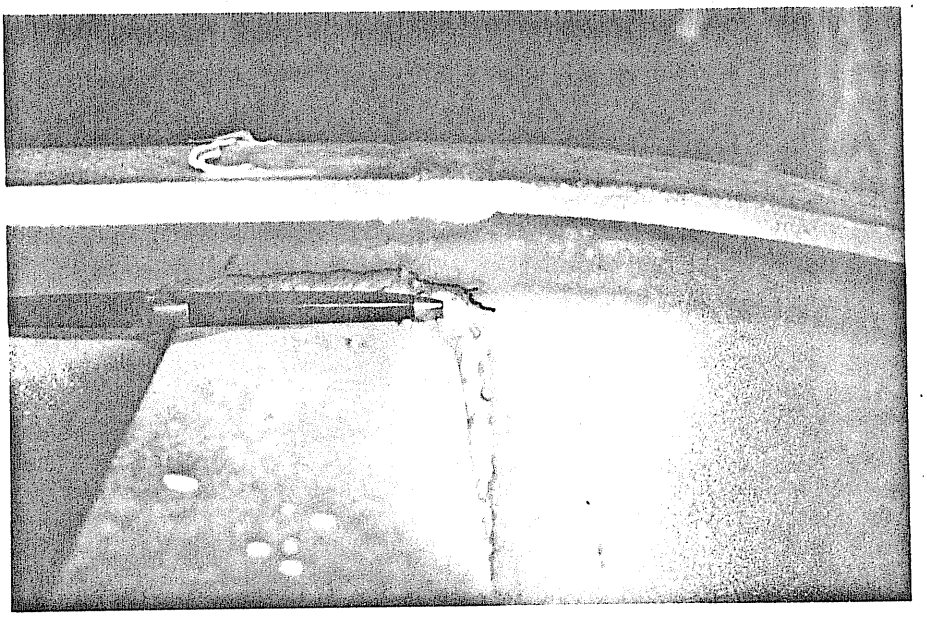

Figure 3.4 Cracks Located on Passenger's Side Beam

CHAPTER IV

SUMMARY AND CONCLUSIONS

In this test program, the behavior of the modified design of curved beams used as frame rails in cementing and fracturing trailers has been measured. These measurements included the relationships between load, vertical deflections, and strains. This section summarizes these results and discusses some of the implications for the fatigue life of the measured frame.

The relationships between applied load and beam deflection at the wire potentiometers was predicted using a plane frame stiffness analysis program. This prediction is shown in Fig. B.3 of Appendix B. In this figure it can be seen that the predicted stiffness of the frame was greater than actual. The most important reason for this overestimation of the frame stiffness is that the analysis failed to account for the tendency of the flanges in the curved beam region to "roll", reducing the stress in the flange at locations away from the web. This reduced flange effectiveness resulted in a smaller effective moment of

inertia for the curved region of the beams which caused the reduced stiffness of the frame.

The distribution of stresses in the flanges of the curved portion of the beams can be seen in the static test results. These results indicate that the toe of the upper flange was much less than fully effective. Strain gages #4 outer, #8 outer, and #12 outer, located on the top of the upper flange next to the beam web, indicated strains of 930, 1214, and 1332 microstrain, respectively, at the maximum load of 46.1 kips (See Figures B.13, B.22 and B.36, Appendix B). At the same load, strain gages #4 inner, #8 inner, and #12 inner, located near the inside toe of the upper flange, indicated strains of only 85, 164, and 207 microstrain, respectively, which represents an average decrease of 87 percent compared to the "outer" gages located near the beam web at the same sections. This reduction of strain in the toes of the top beam flanges is due to the out-of-plane deflections of the unsymmetric flanges.

The static test also indicated that the toe of the bottom flange was almost fully effective. Strain gage #1 mid, located on the bottom of the lower flange next to the web, indicated a strain of 1130 microstrain at a load of 46.1 kips. At the same load level, strain gages #1 outer, and #1 inner, located near the outer and inner toes of the lower flange, respectively, indicated strains of 1075, and

952 microstrain, respectively. This uniform distribution of strains across the flange width is due to the symmetry of the lower flange about the beam web.

During the fatigue test, cracks were first noticed at 690,000 cycles in an area where direct bending stresses (due to in-plane bending of the frame rails) are compressive and large tensile stresses are generated due to the "rolling" of the top flanges. These cracks grew slowly compared to cracks in the previous test frame and had not penetrated the beam webs when the test was completed at 1,000,000 cycles. No cracks were observed in the bottom half of the beam, where "rolling" of the flange was eliminated by the symmetric bottom flange design. The cracks observed were the result of the concentrated support to resist rolling provided to the web by the cross member resulting in a stress concentration. The location of these cracks were in good agreement with diagrams provided by Halliburton Services, indicating the most highly stresses points of the trailer frame.

Maximum stresses calculated from the strain gage data are presented in Tables 4.1 and 4.2. These tables provide peak values of stresses calculated from strain gage readings taken during the static test.

Table 4.1 contains the maximum values of stress calculated from the uniaxial strain gages installed on the

beam flanges in the locations shown in Fig. 2.8. From this data, it can be seen that the maximum stress is largest near the beam web at gage #12 outer and is smaller at each strain gage located farther from the beam web (at strain gages #4, #8, and #12 inner). The bottom flange is subjected to a uniform stress, as indicated from strain readings at locations 1 & 9, due to its symmetry about the beam web. Only small stresses are present in the bottom flange at location 9, due to the sharp bend in the flange plate at this location.

Table 4.2 contains the maximum values of equivalent uniaxial stress calculated for each rosette using the Von Mises yield criterion. The location of the elements of these rosettes were shown previously in Figures 2.6 and 2.7. The largest equivalent stress in this table occurs at the rosette 13 outer which consists of 13-90°, 45°, and 0°, outer.

From the large number of cycles before the first crack was observed and the slow growth rate as compared to the frame tested previously, it is concluded that this frame design is significantly better than the previous design. The elimination of bottom flange rolling by the symmetric design of the bottom flange about the beam web was a major contributor to this improvement.

The cracks which occurred in this specimen were

primarily caused by the "rolling" of the top curved flange. If additional improvements in fatigue life are needed, reductions in the amount of "rolling" in the top curved flange should be attempted, either by direct braces to the top flange, manufacture of a symmetric top flange, or other methods.

TABLE 4.1

MAXIMUM UNIAXIAL STRESSES

Strain Gage Number	Uniaxial Stress (ksi) (Load = 46.1 k)
1, outer	32.3
1, mid	33.9
1, inner	28.6
5, mid	18.5
9, outer	-4.3
9, mid	-2.1
9, inner	-7.5
4, outer	27.9
4, inner	-2.6
8, outer	-36.4
8, inner	-4.9
12, outer	-39.9
12, inner	-6.2

TABLE 4.2

MAXIMUM VON MISES STRESSES

Rosette Strain Gage Number	Von Mises Stress (ksi) (Load = 46.1 k)
2-90°, 45°, 0°	9.2
3-90°, 45°, 0°	26.2
6-90°, 45°, 0°	15.0
7-90°, 45°, 0°	32.5
10-90°, 45°, 0°	45.8
11-90°, 45°, 0° (Outer)	61.5
11-90°, 45°, 0° (Inner)	26.9
13-90°, 45°, 0° (Outer)	65.3
13-90°, 45°, 0° (Inner)	25.1

APPENDIX A

SPECIMEN DIMENSIONS, PROPERTIES, AND ANALYSIS RESULTS

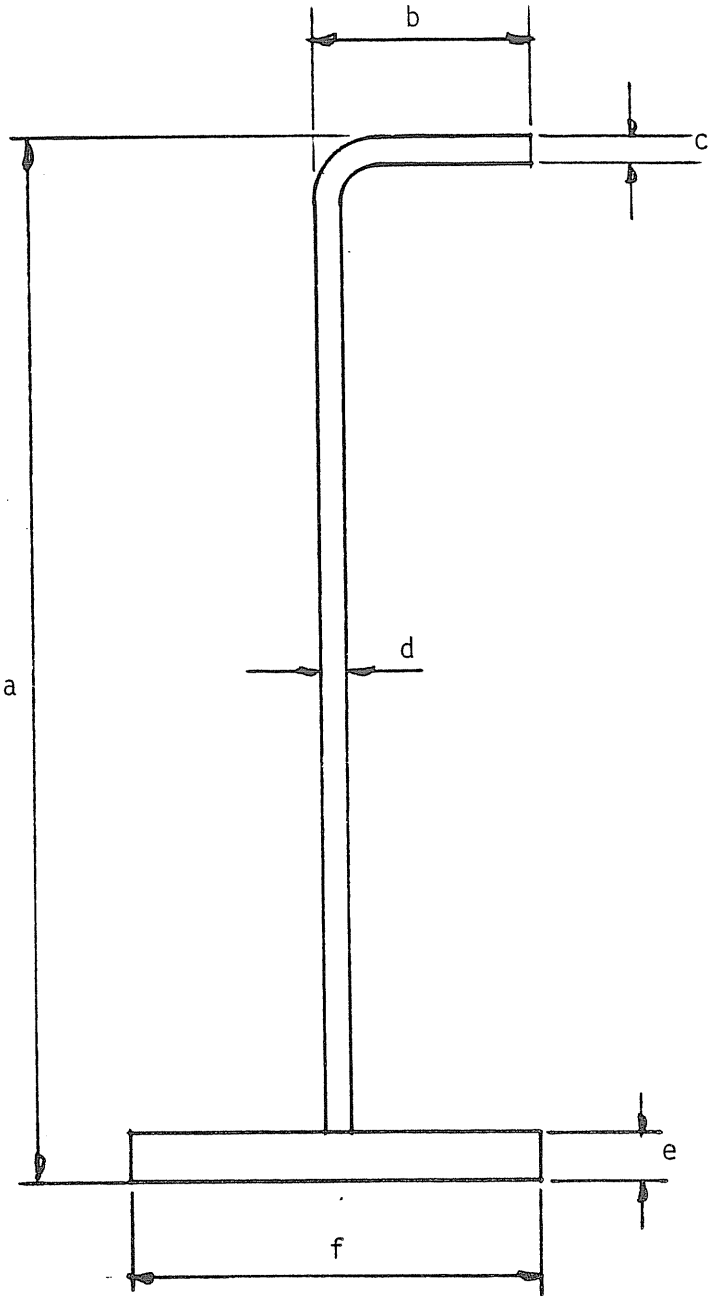

Figure A.1 Dimensions Measured at Each Cross Section

Table A.1

Cross Section Dimensions

Dimensions (inches)						
Cross Sect.	a	b	c	d	e	f
1	12.375	3.375	0.364	0.364	1.125	4.1875
2	12.5625	3.375	0.366	0.366	1.125	4.1875
3	12.1875	3.375	0.364	0.364	0.765	4.1875
4	14.250	3.375	0.362	0.362	0.772	4.1875
5	15.750	3.375	0.361	0.361	0.761	4.1875
6	18.500	3.4375	0.337	0.363	0.761	4.1875
7	19.750	3.4375	0.338	0.363	0.770	4.1875
8	22.750	3.4375	0.335	0.363	0.772	4.1875
9	20.000	3.375	0.366	0.366	0.769	4.1875
10	20.250	3.375	0.368	0.368	0.764	4.1875
11	20.1875	3.375	0.366	0.366	0.738	4.1875
12	17.8125	3.375	0.395	0.395	0.770	4.1875
13	15.750	3.375	0.393	0.393	0.769	4.1875
14	13.500	3.375	0.393	0.393	1.1875	4.1875

Table A.2

Cross Section Properties

Cross Section	Area (in^2)	Centroid* Location (in)	Moment of Inertia (in^4)
1	9.90	4.41	202.3
2	9.99	4.49	210.6
3	8.46	4.88	176.4
4	9.20	5.79	257.7
5	9.69	6.49	326.9
6	10.66	7.71	480.9
7	11.15	8.27	567.7
8	12.24	9.67	806.6
9	11.36	8.46	595.2
10	11.48	8.61	614.69
11	11.31	8.63	601.9
12	11.13	7.59	468.3
13	10.28	6.62	344.8
14	10.98	4.92	265.6

*From bottom of section

Table A.3

Stiffness Analysis Results
(Load = 10.0 kips)

Member	Connecting Sections	Axial Load (kips)	Shear (kips)	Moment (kip-ft)
1	1 2	0.05 -0.05	-6.85 6.85	0.00 -6.85
2	2 3	0.07 -0.07	-6.85 6.85	6.85 -27.41
3	3 4	0.30 -0.30	-6.85 3.65	27.41 -36.09
4	4 5	2.56 -2.56	-2.60 2.60	36.09 -38.53
5	5 6	0.39 -0.39	-3.63 3.63	38.53 -40.66
6	6 7	1.59 -1.59	-3.29 3.29	40.66 -42.79
7	7 8	3.20 -3.20	-1.76 1.76	42.79 -44.31
8	8 9	0.54 -0.54	-3.61 3.61	44.31 -46.44
9	9 10	0.00 0.00	-3.65 -3.15	46.44 -38.28
10	10 11	0.00 0.00	3.15 -3.15	38.28 -19.01
11	11 12	0.19 -0.19	3.14 -3.14	19.01 -13.11
12	12 13	0.14 -0.14	3.14 -3.14	13.11 - 6.82
13	13 14	0.07 -0.07	3.15 -3.15	6.82 0.00

APPENDIX B

STATIC TEST RESULTS

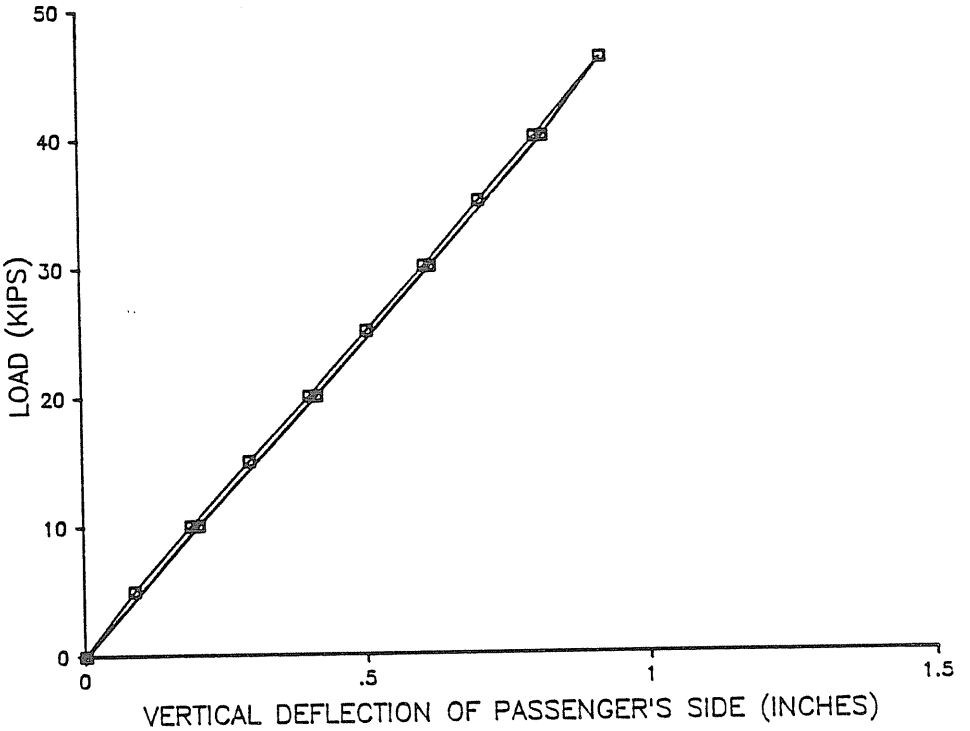

Figure B.1

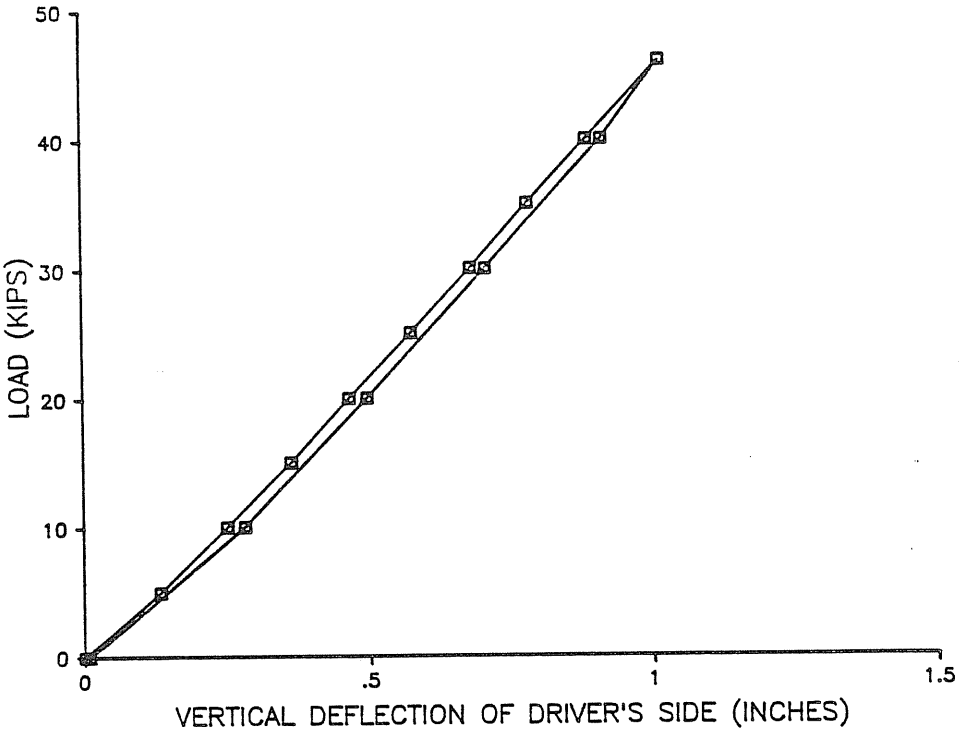

Figure B.2

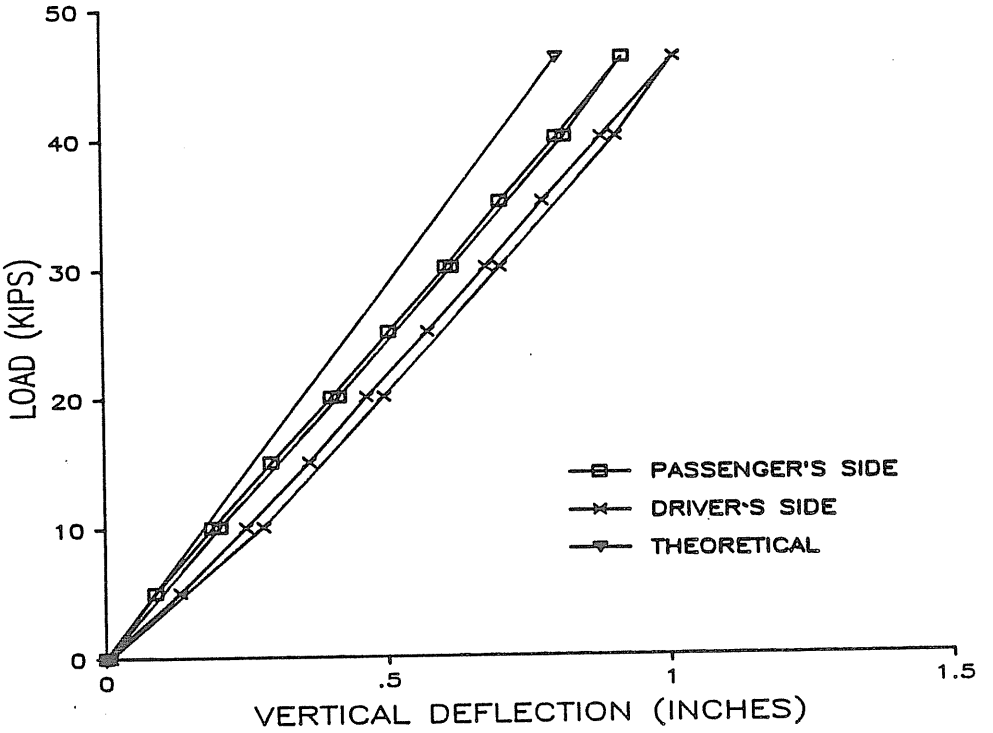
50
40
30
20
10
0
LOAD (KIPS)
0
.5
1
1.5
VERTICAL DEFLECTION (INCHES)
PASSENGER'S SIDE
DRIVER'S SIDE
THEORETICAL

Figure B.3

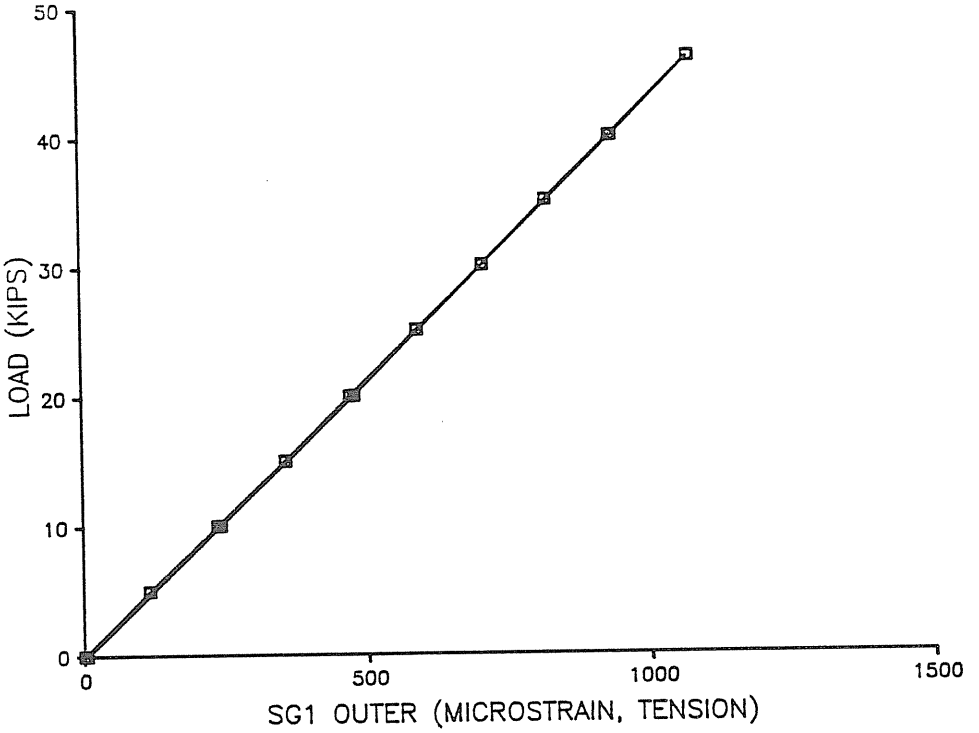

Figure B.4

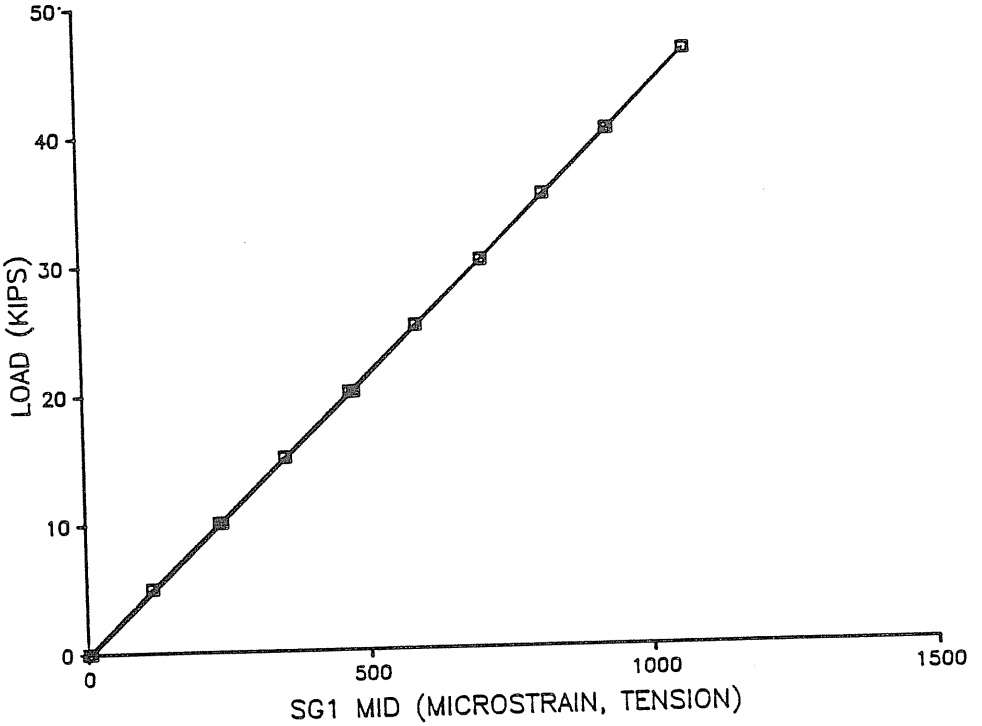

Figure B.5

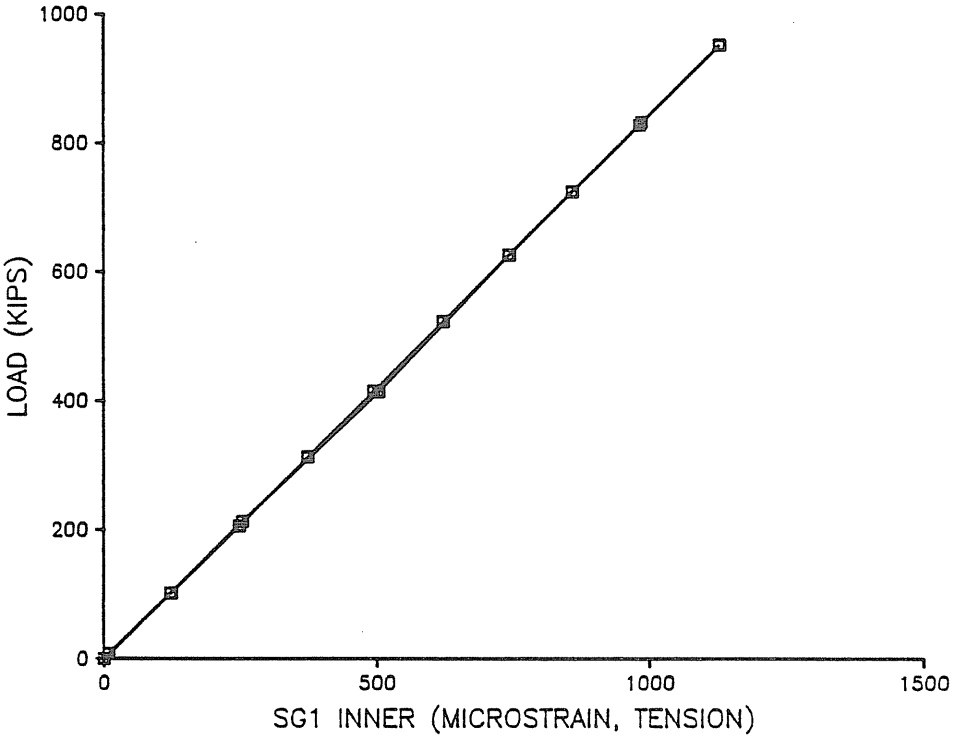

Figure B.6

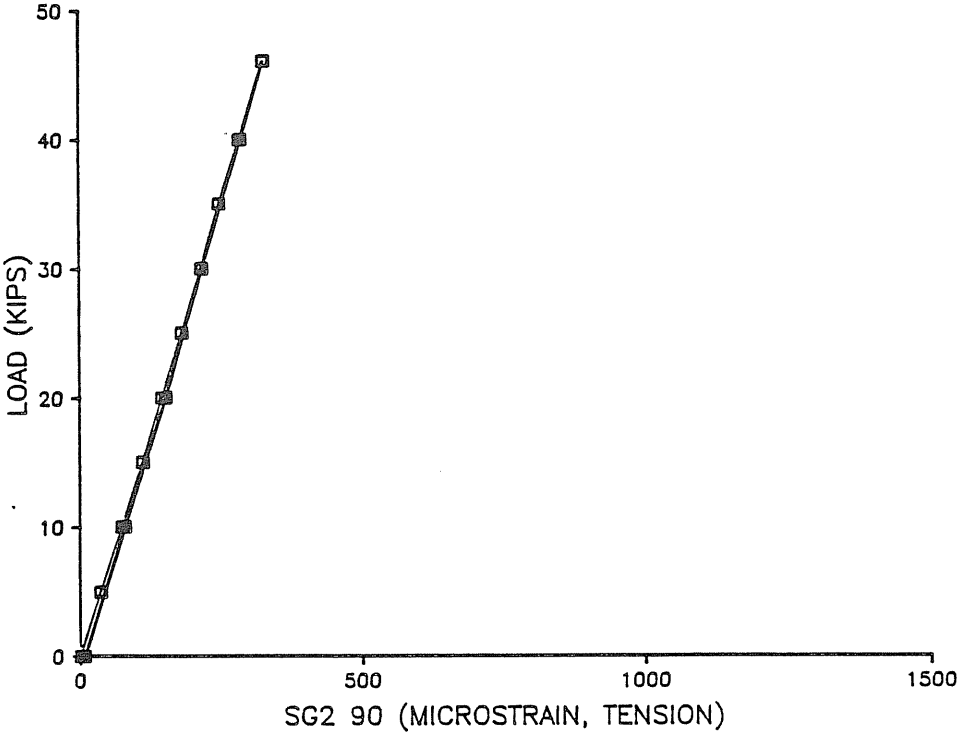

Figure B.7

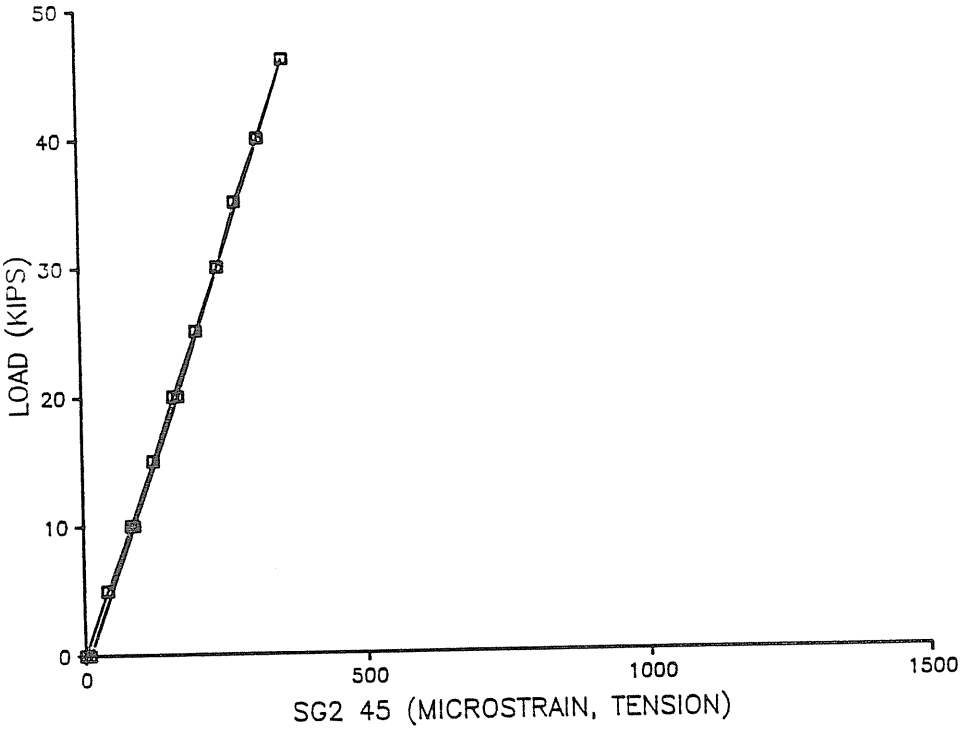

Figure B.8

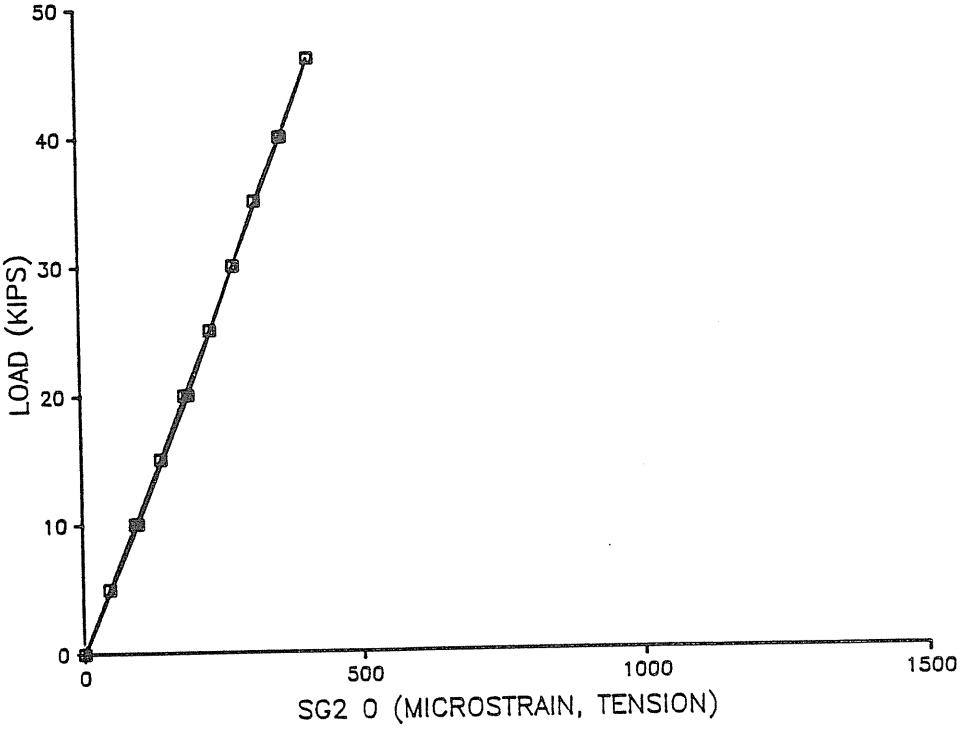

Figure B.9

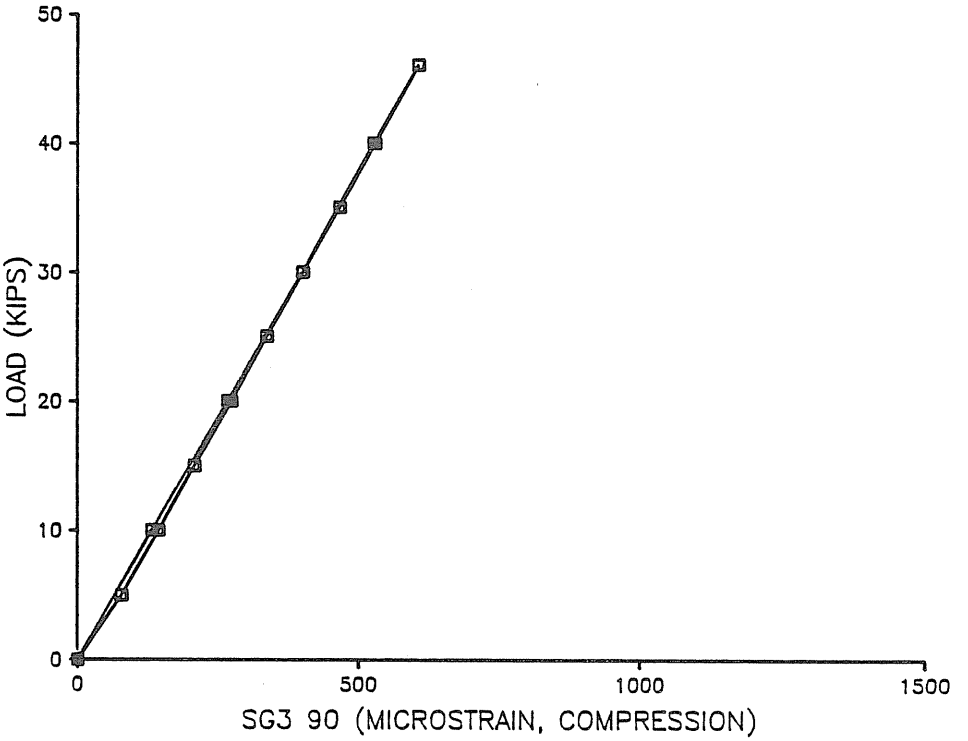

Figure B.10

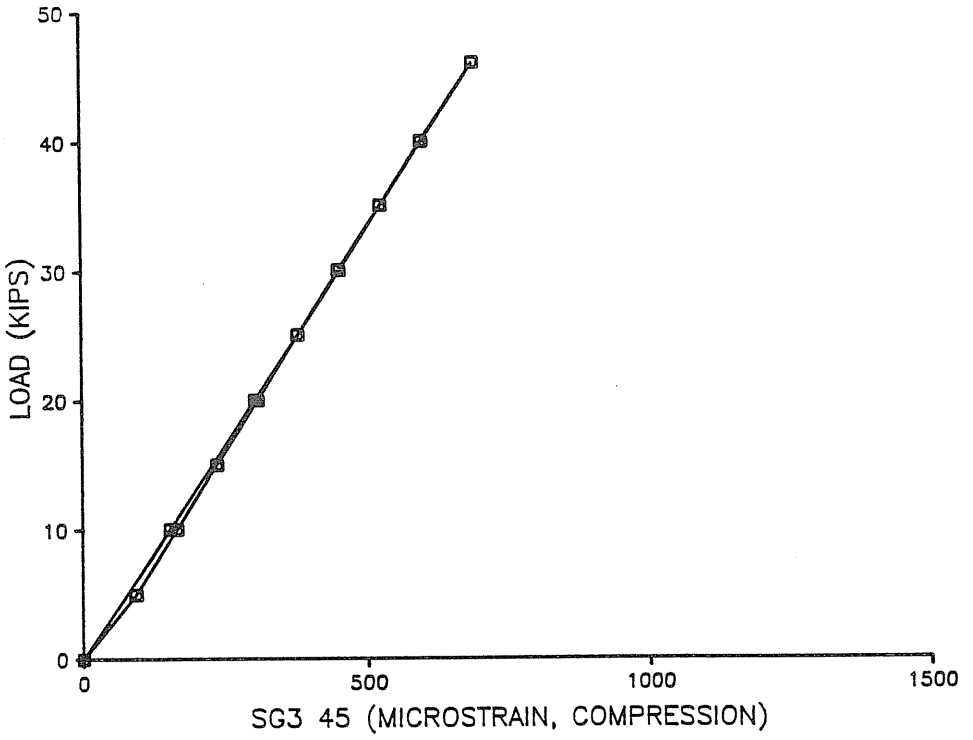

Figure B.11

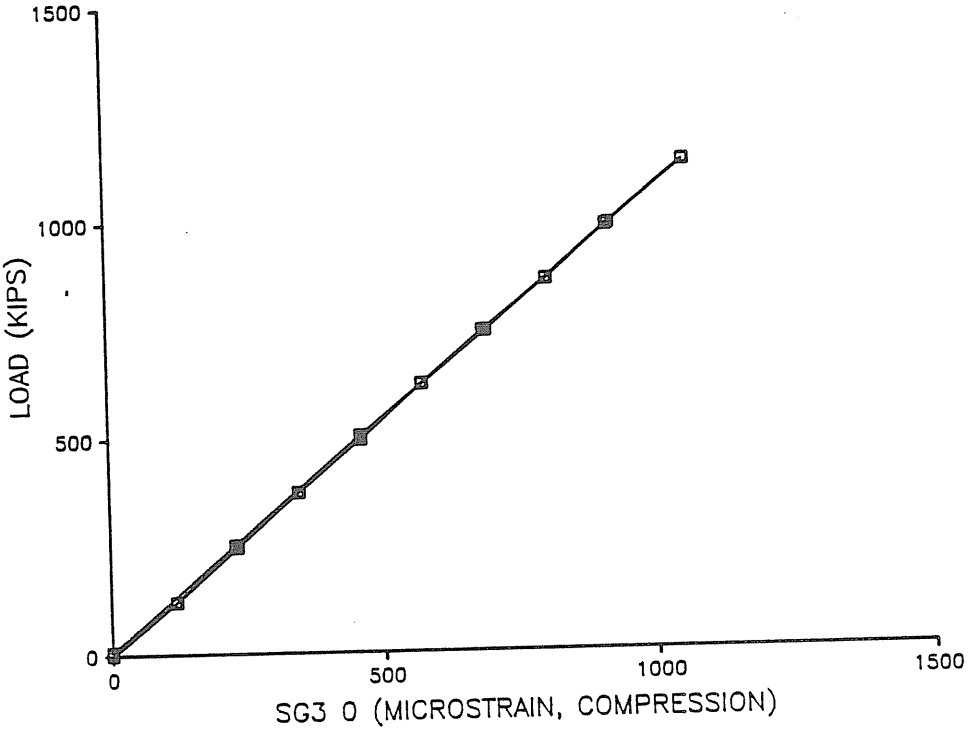

Figure B.12

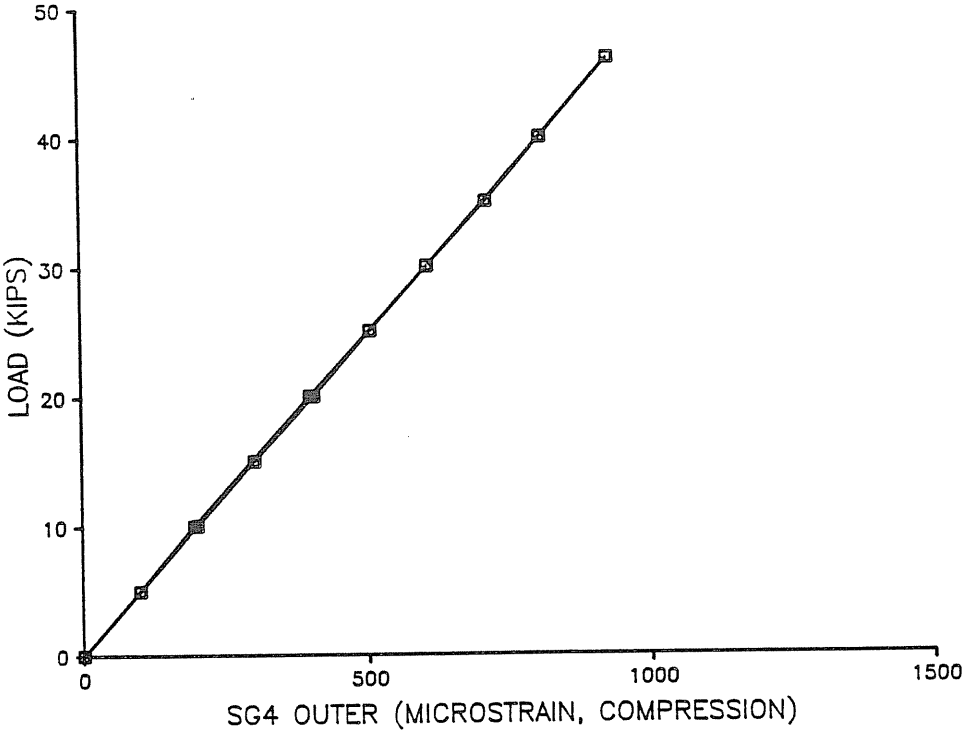

Figure B.13

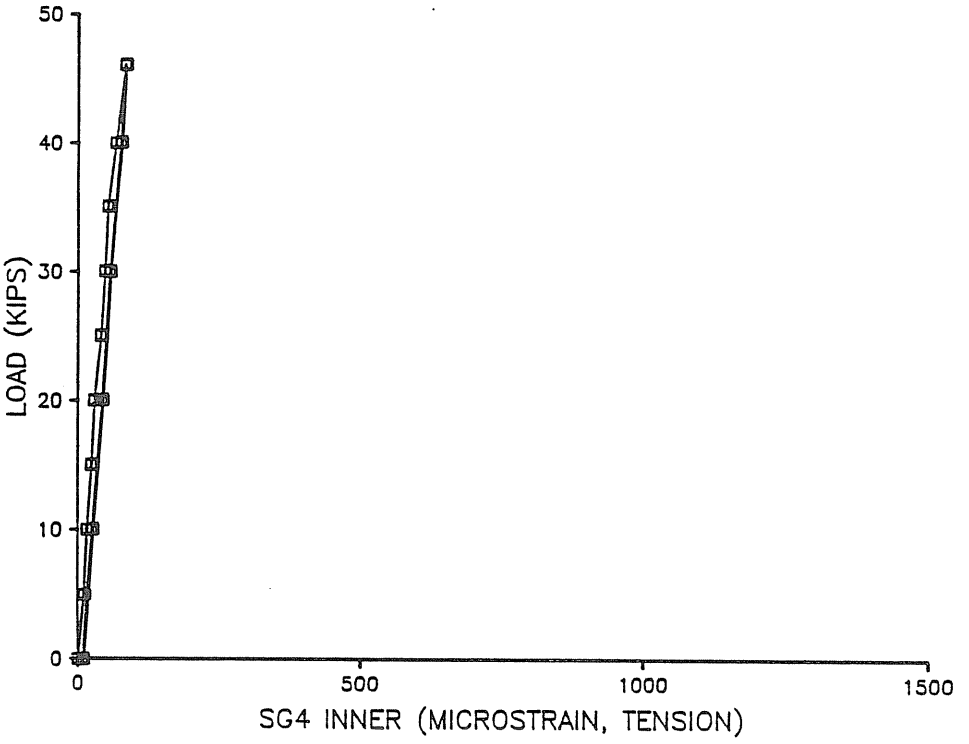

Figure B.14

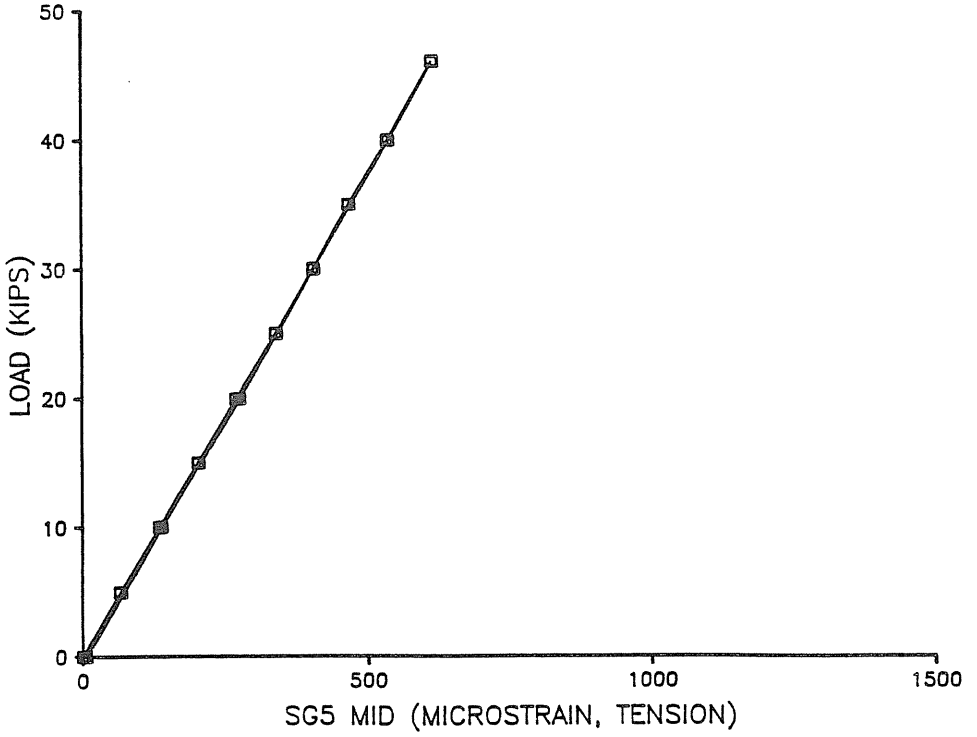

Figure B.15

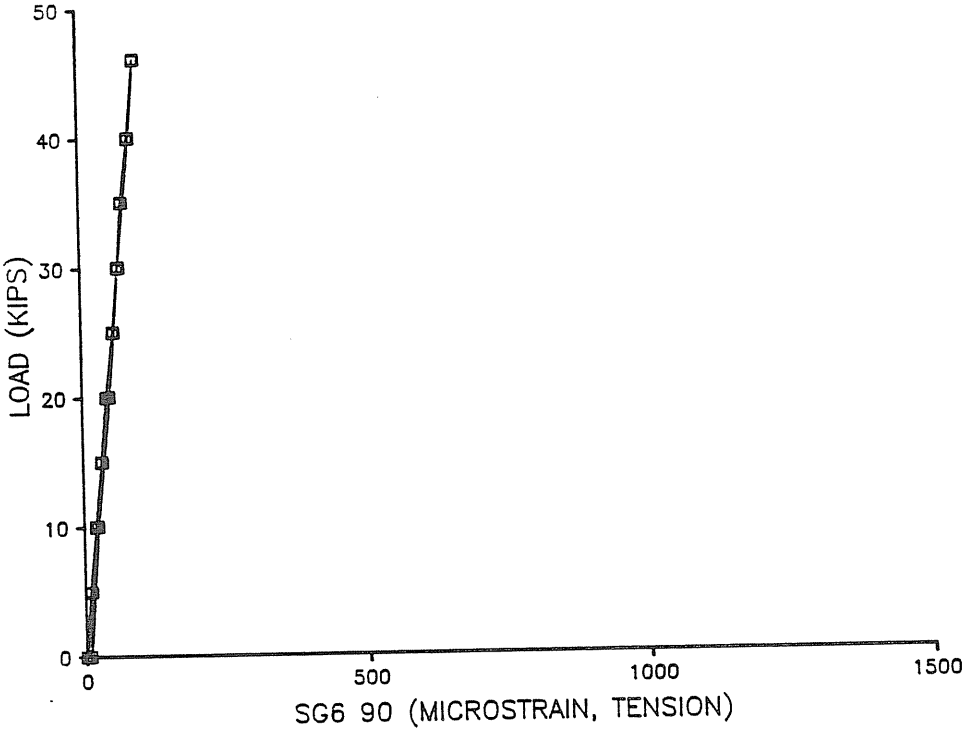

Figure B.16

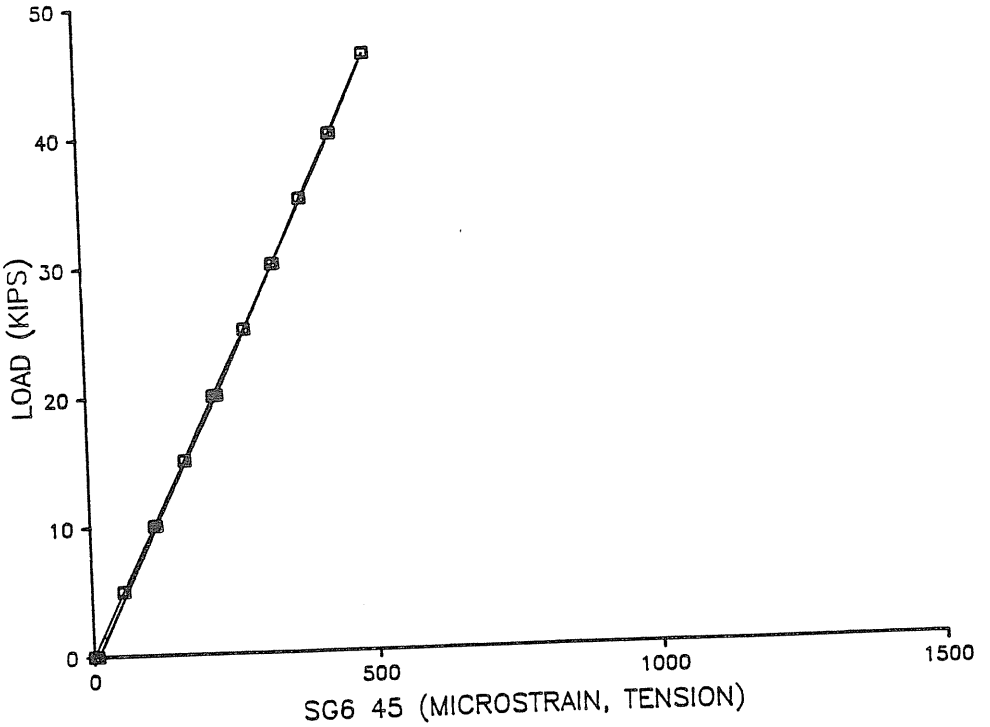

Figure B.17

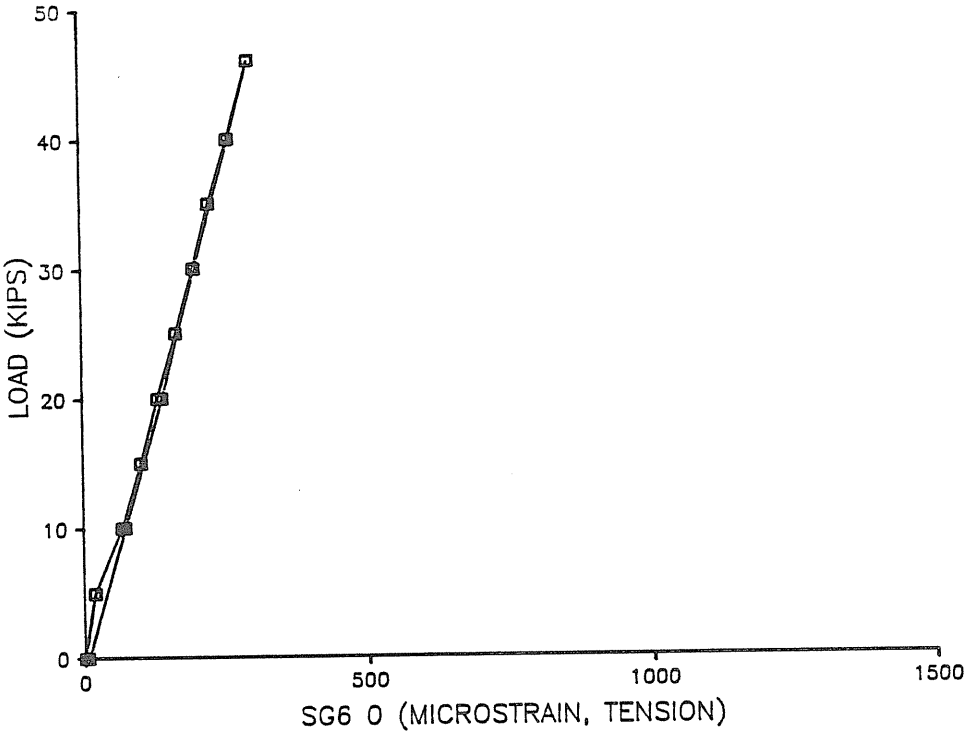

Figure B.18

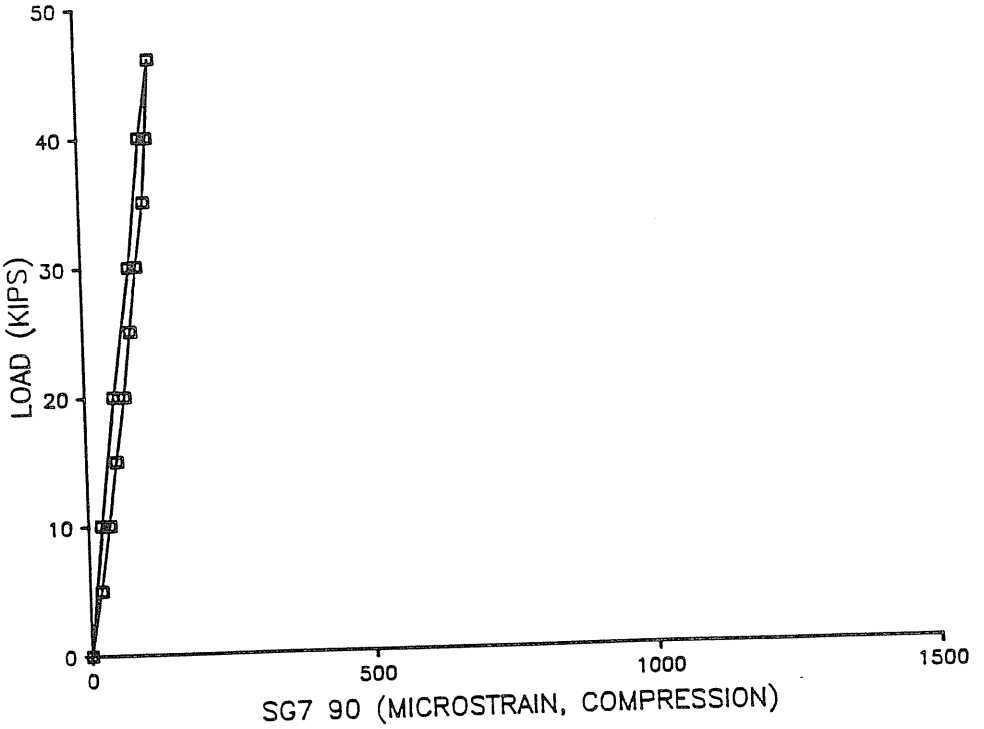

Figure B.19

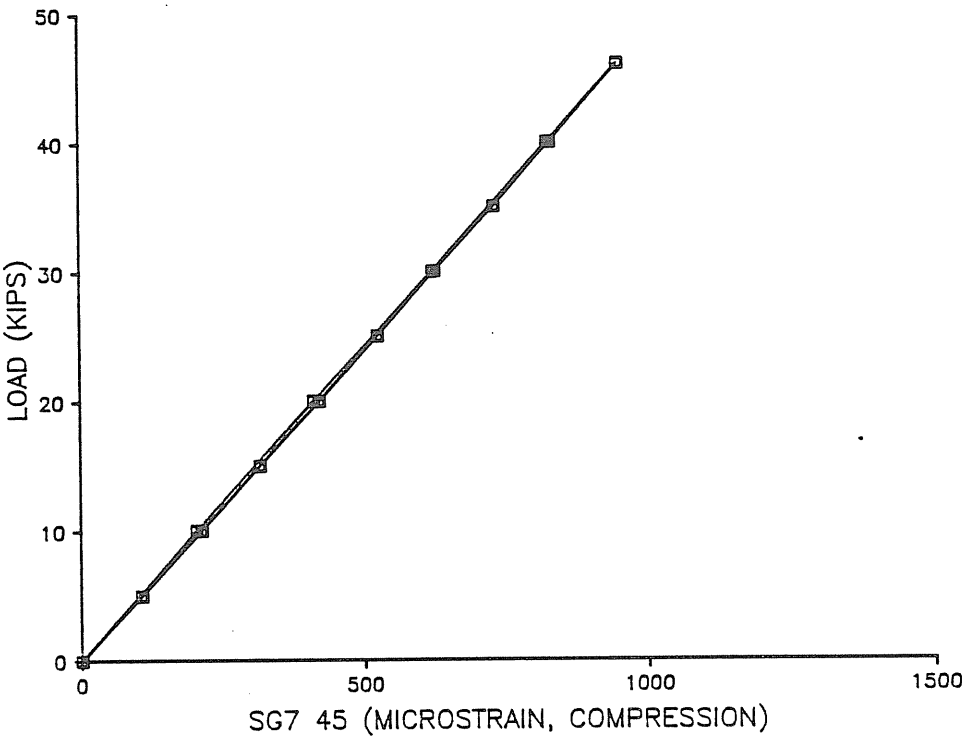

Figure B.20

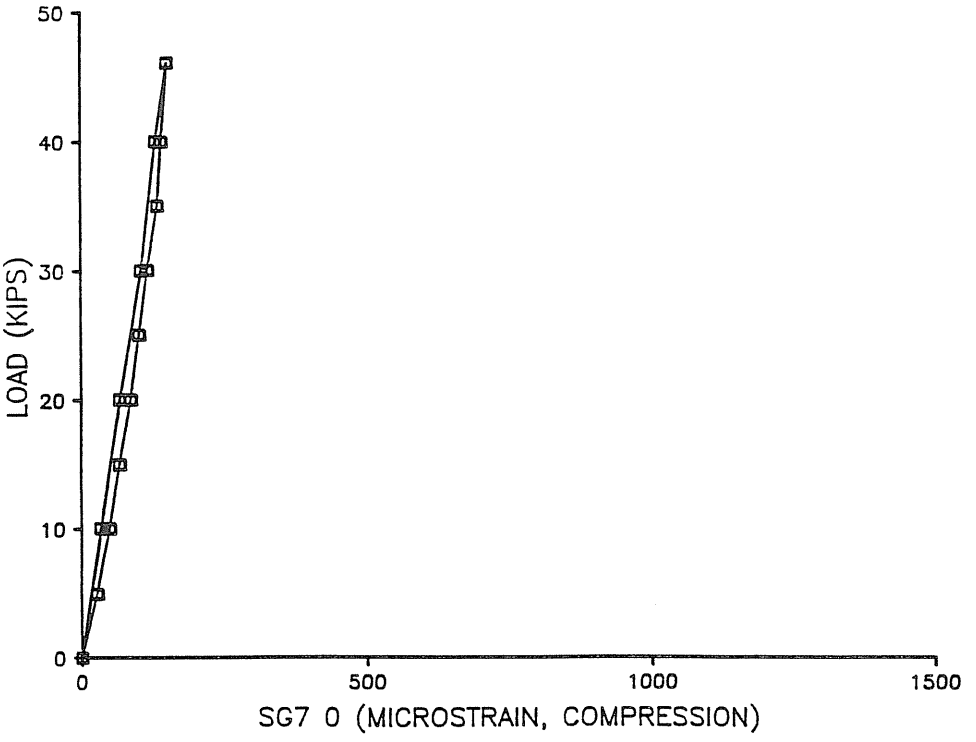

Figure B.21

Figure B.22

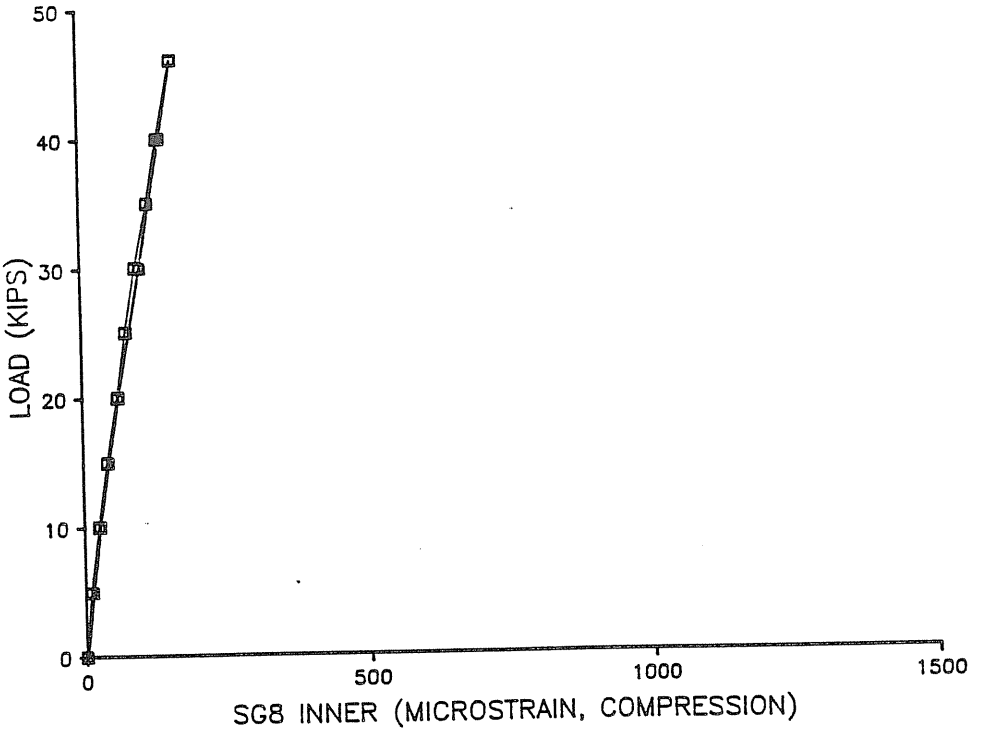

Figure B.23

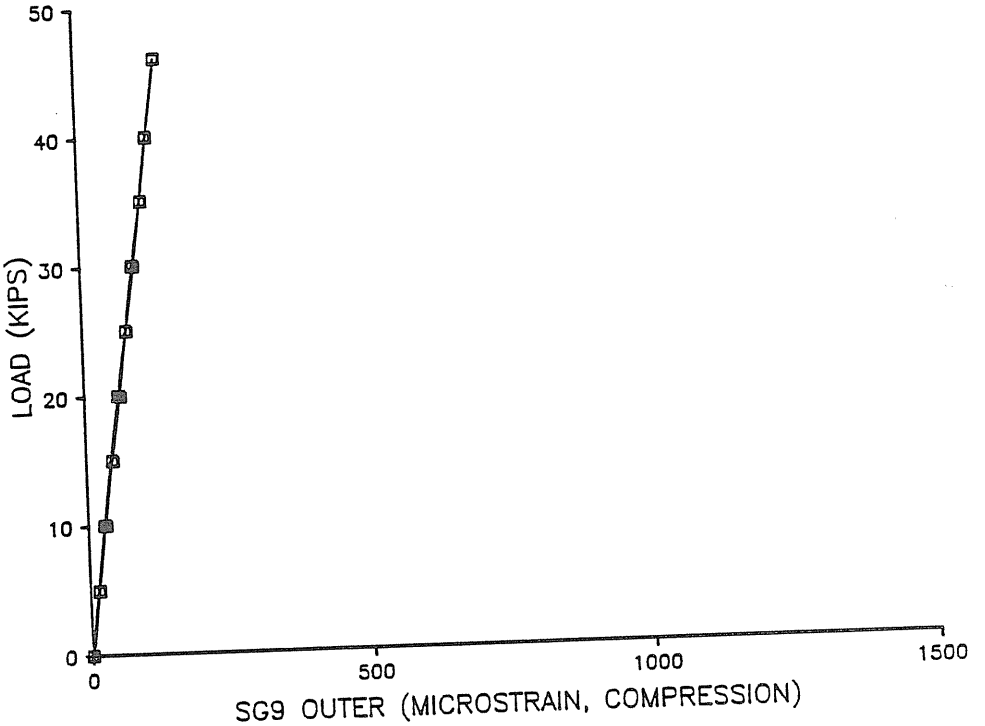

Figure B.24

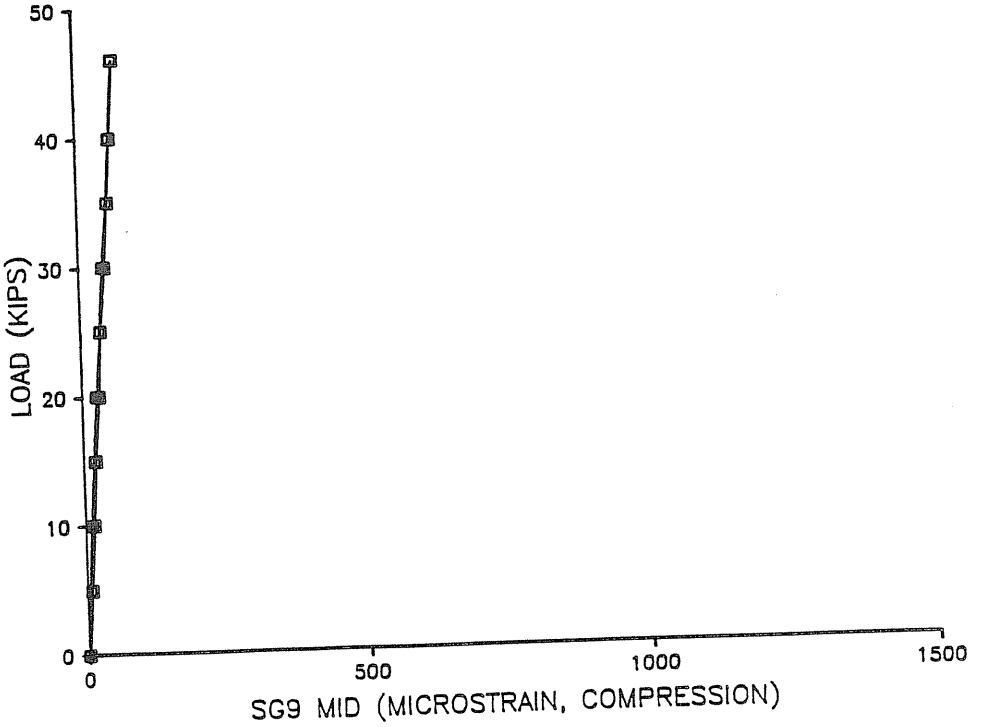

Figure B.25

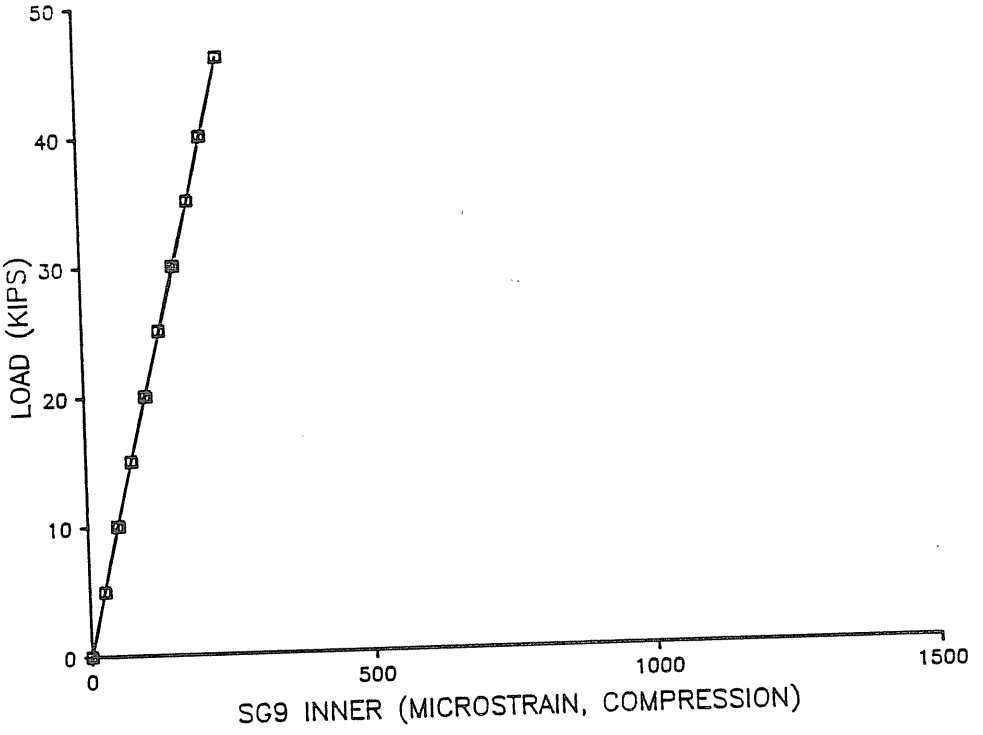

Figure B.26

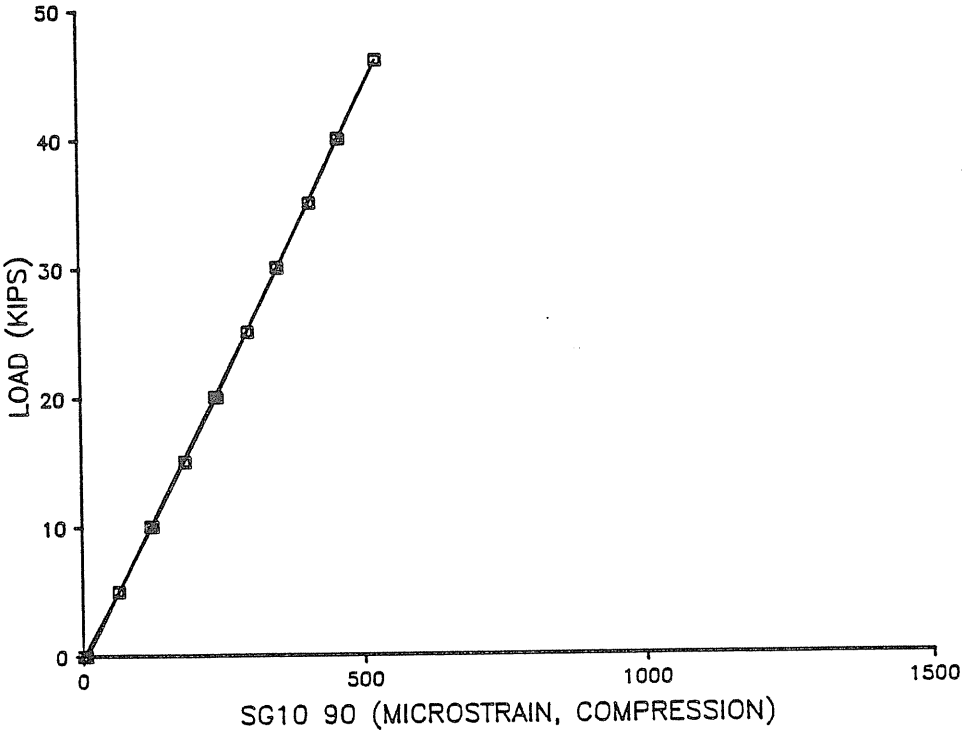

Figure B.27

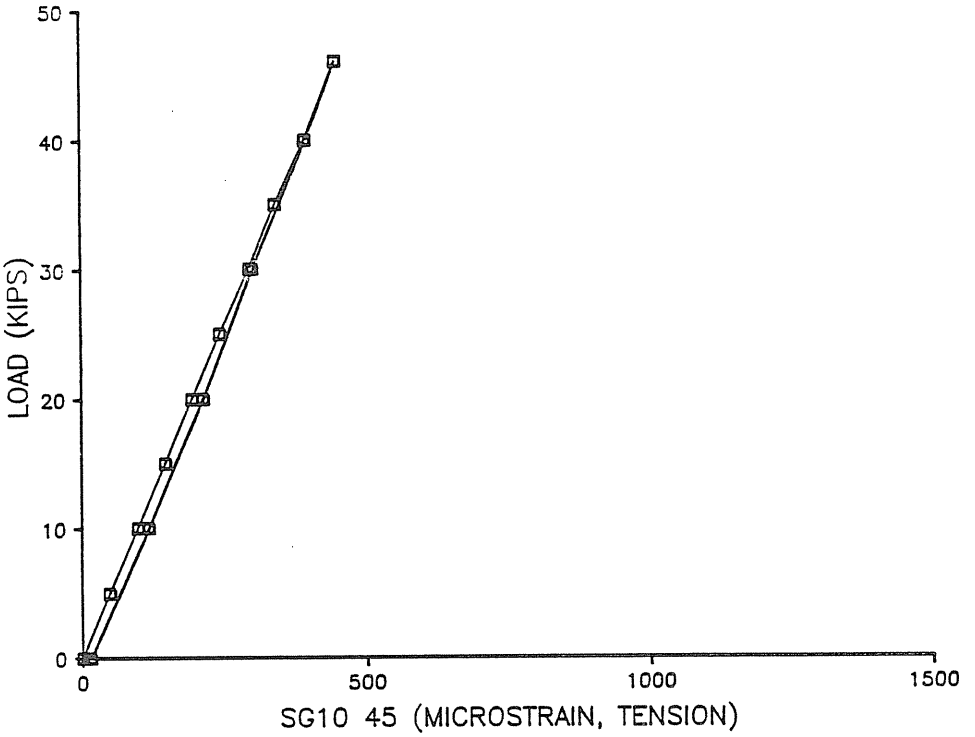

Figure B.28

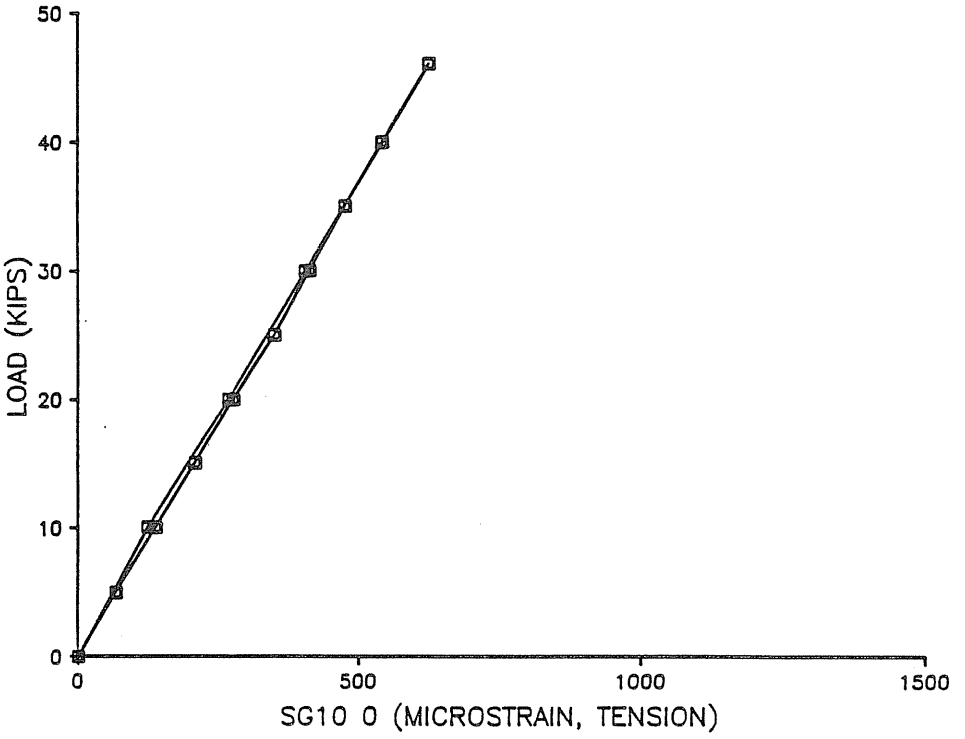

Figure B.29

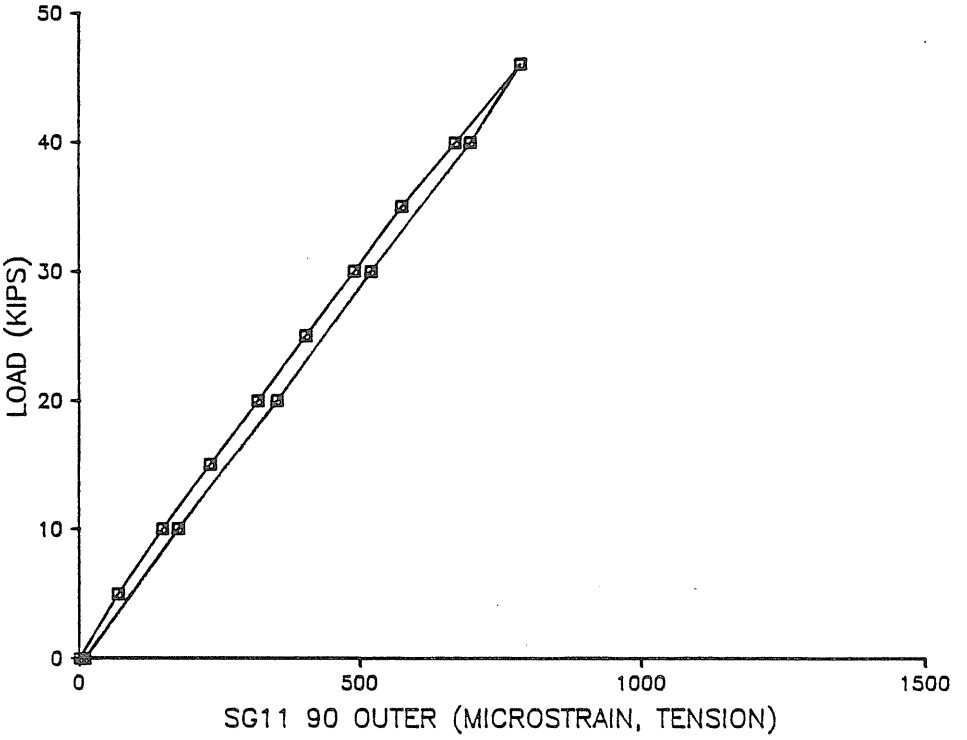

Figure B.30

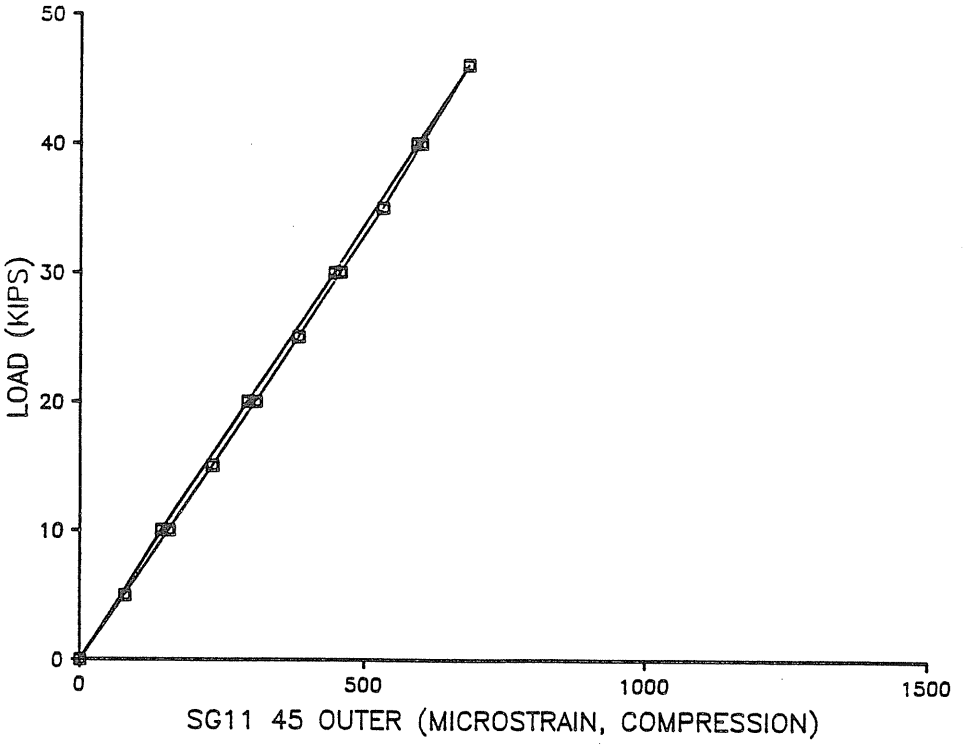

Figure B.31

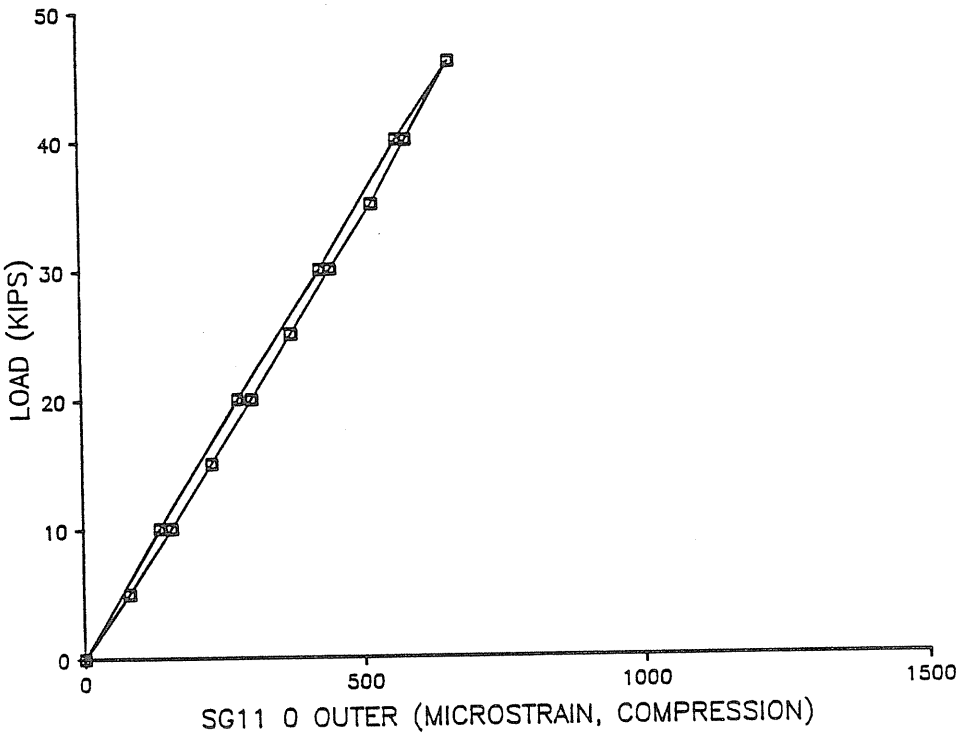

Figure B.32

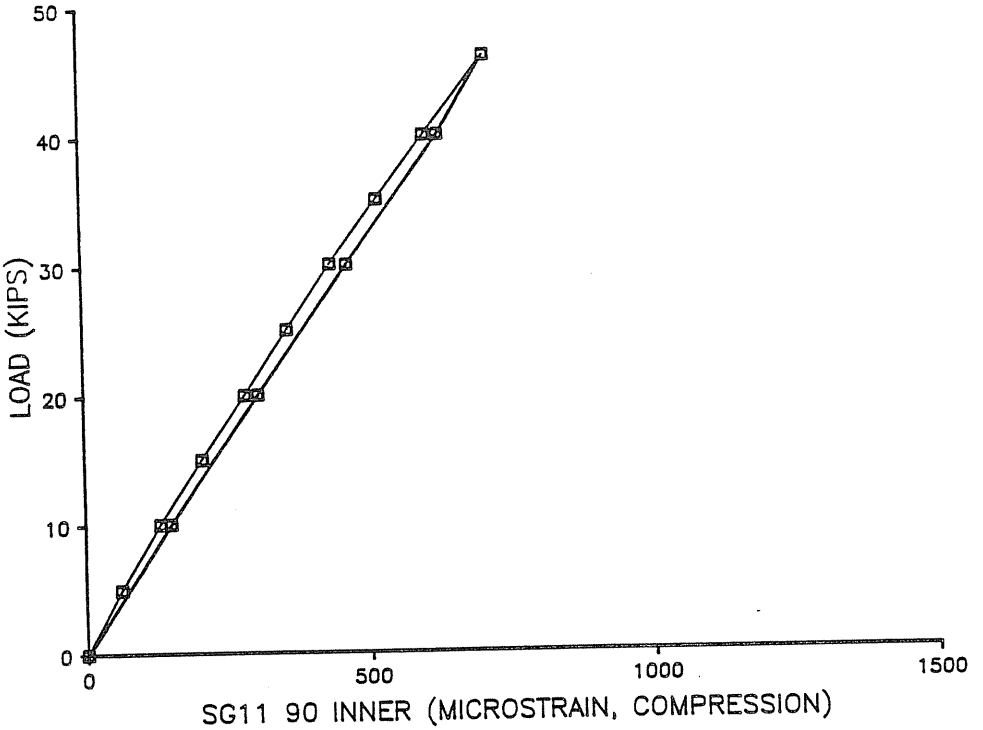

Figure B.33

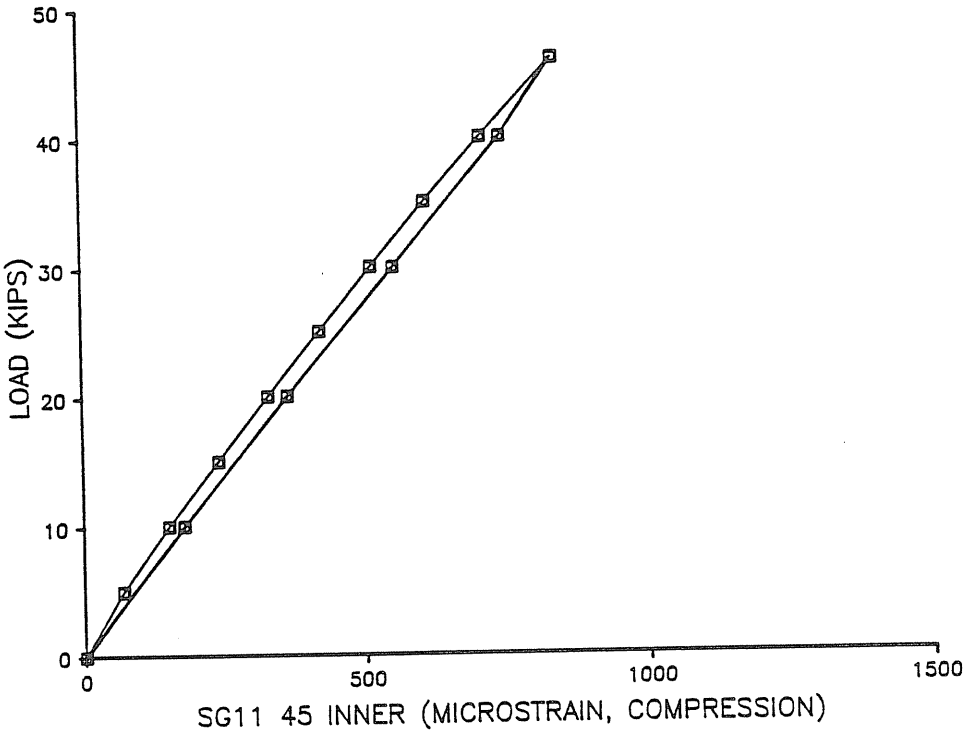

Figure B.34

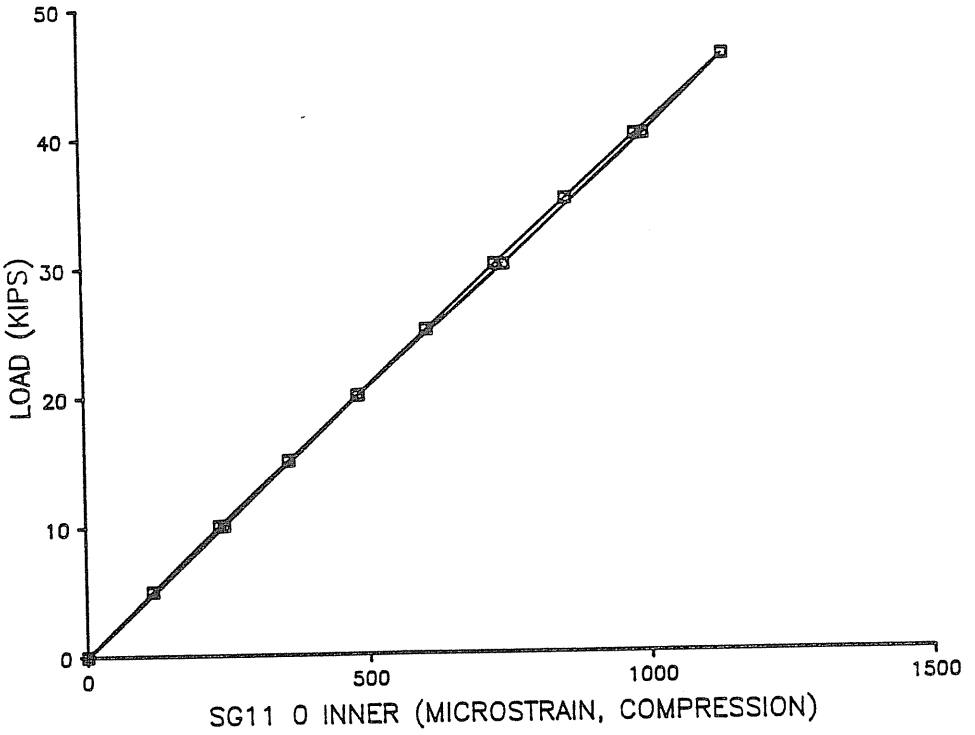

Figure B.35

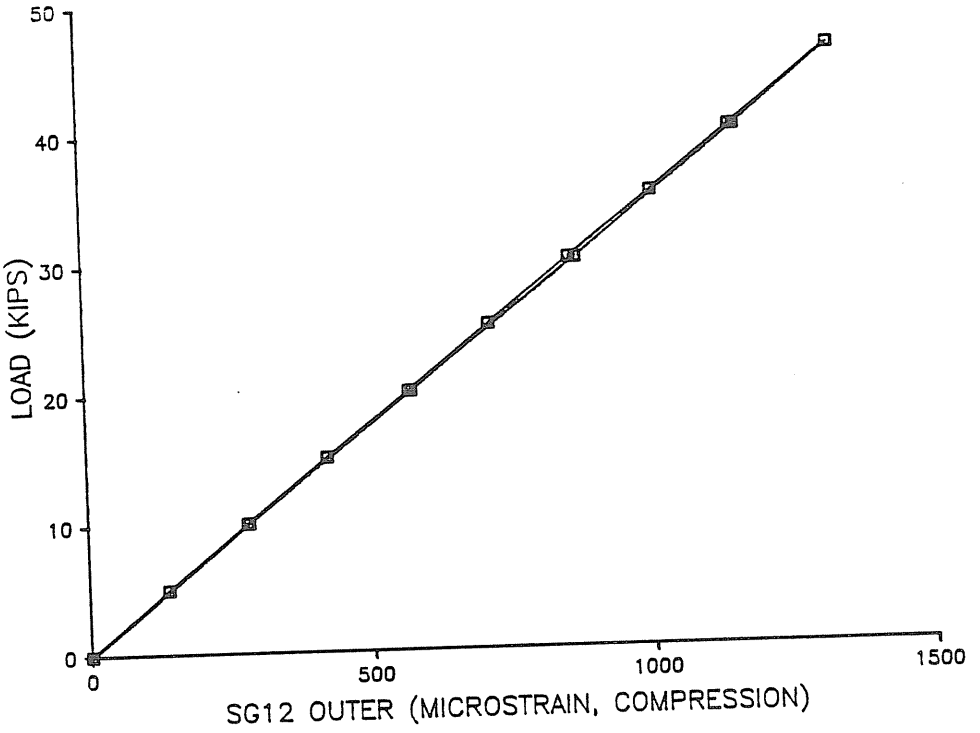

Figure B.36

Figure B.37

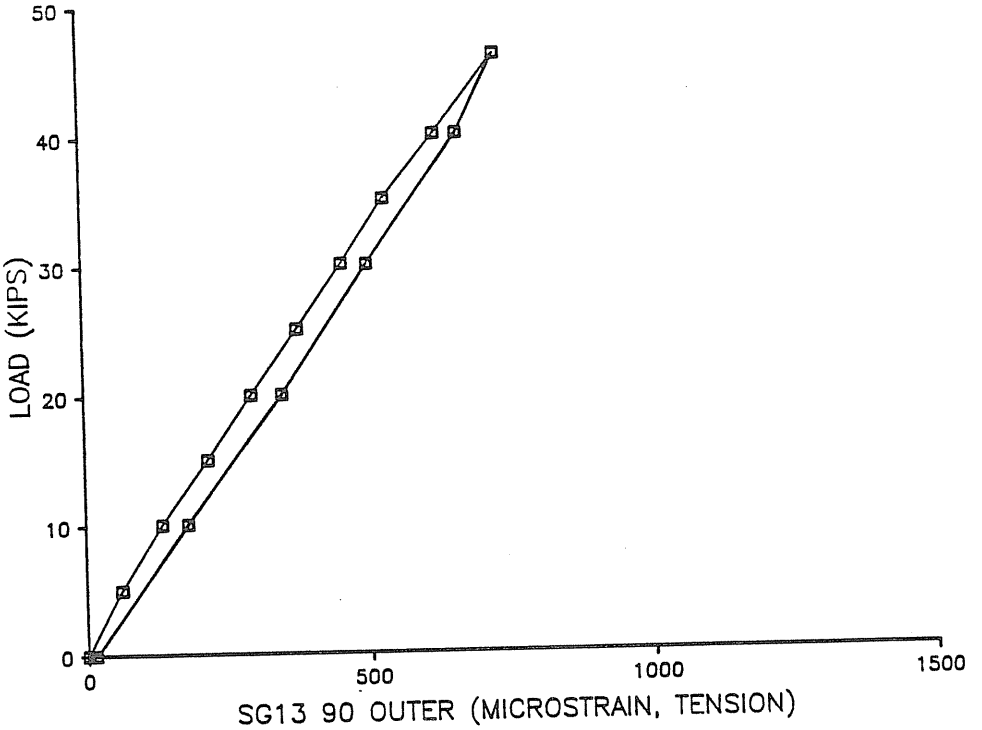

Figure B.38

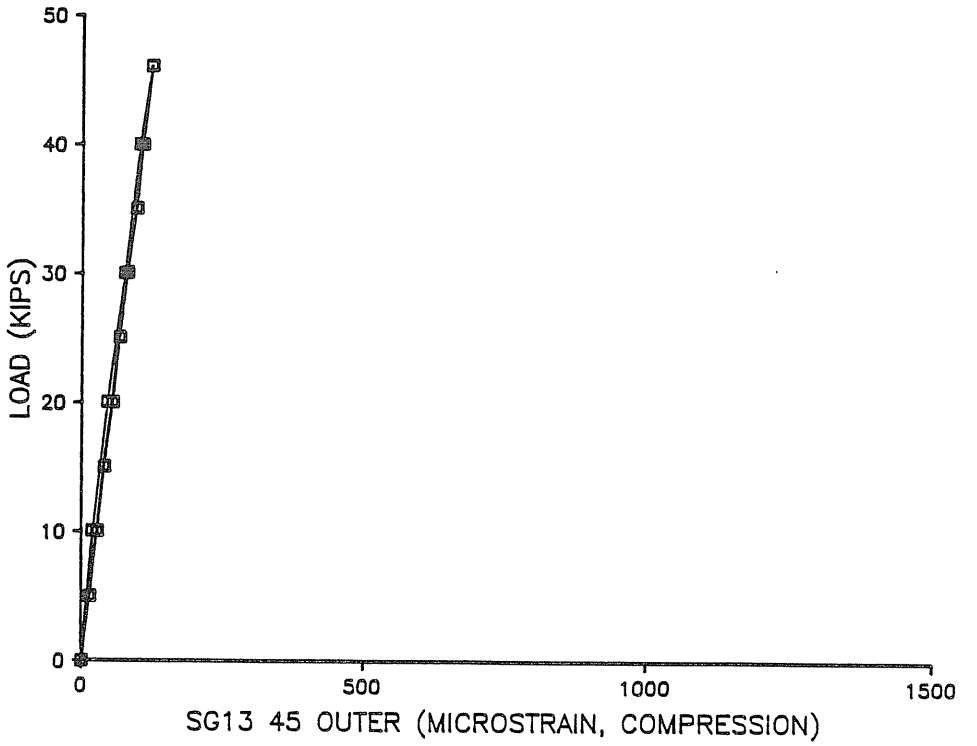

Figure B.39

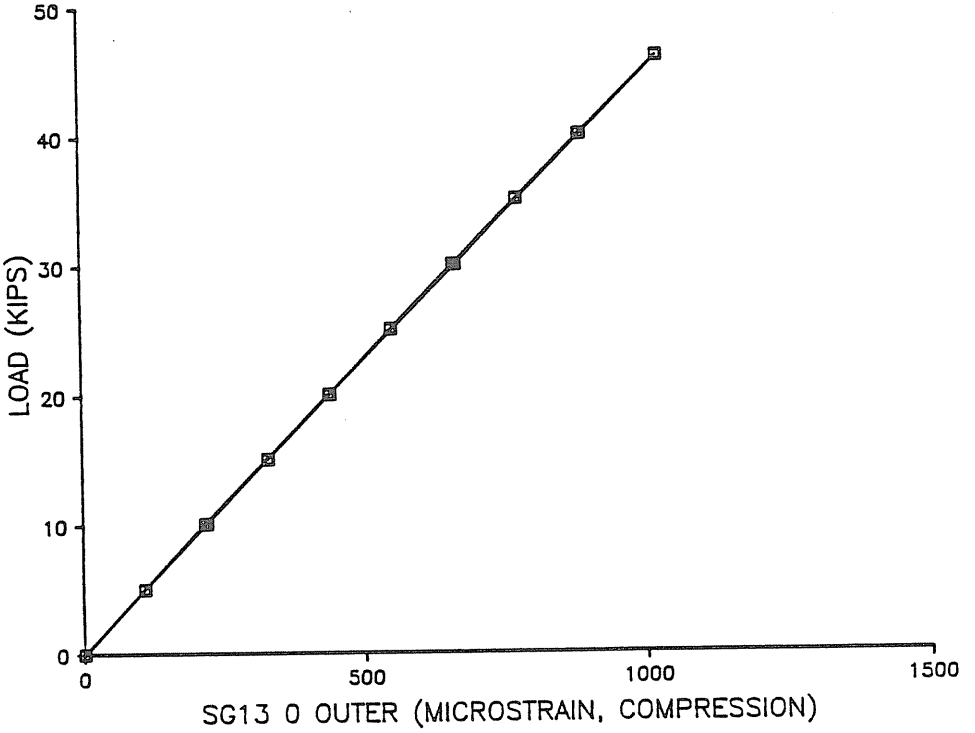

Figure B.40

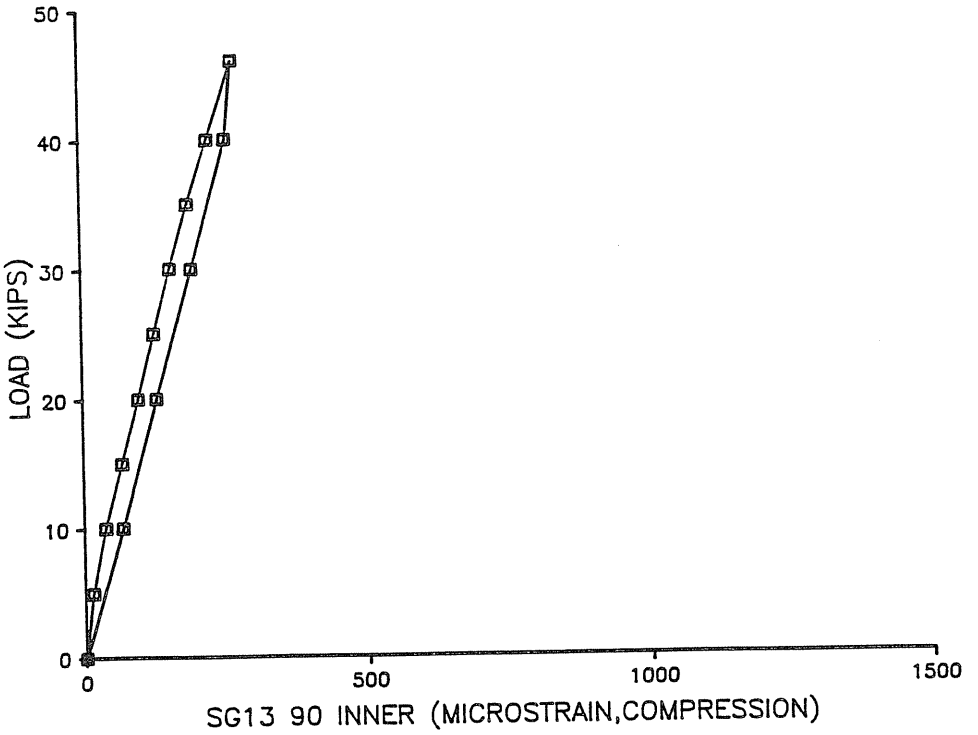

Figure B.41

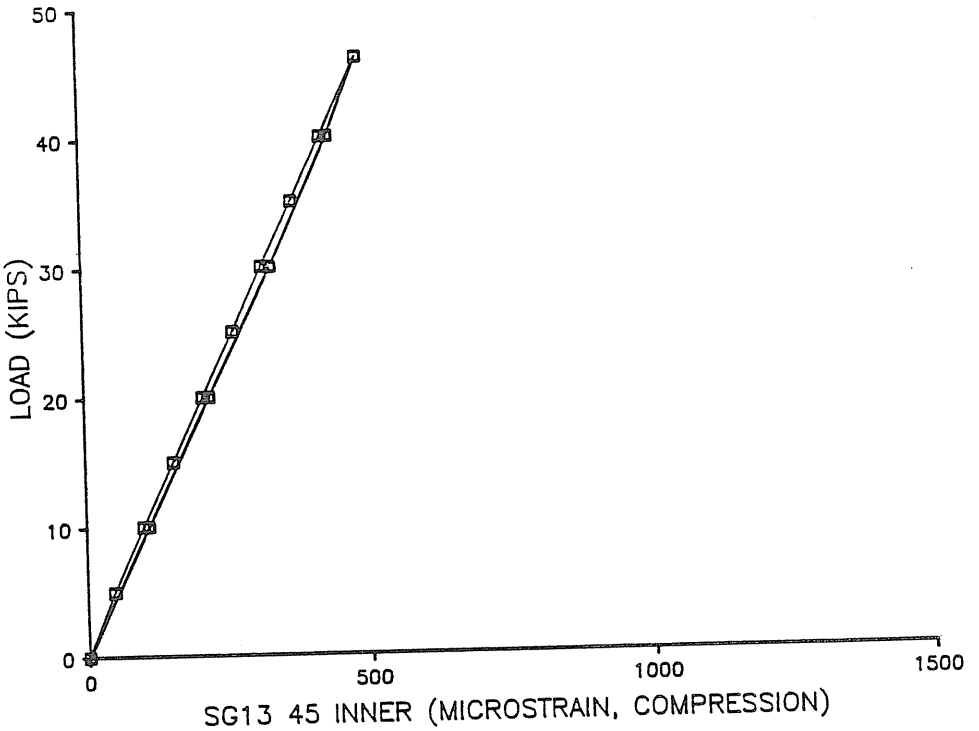

Figure B.42

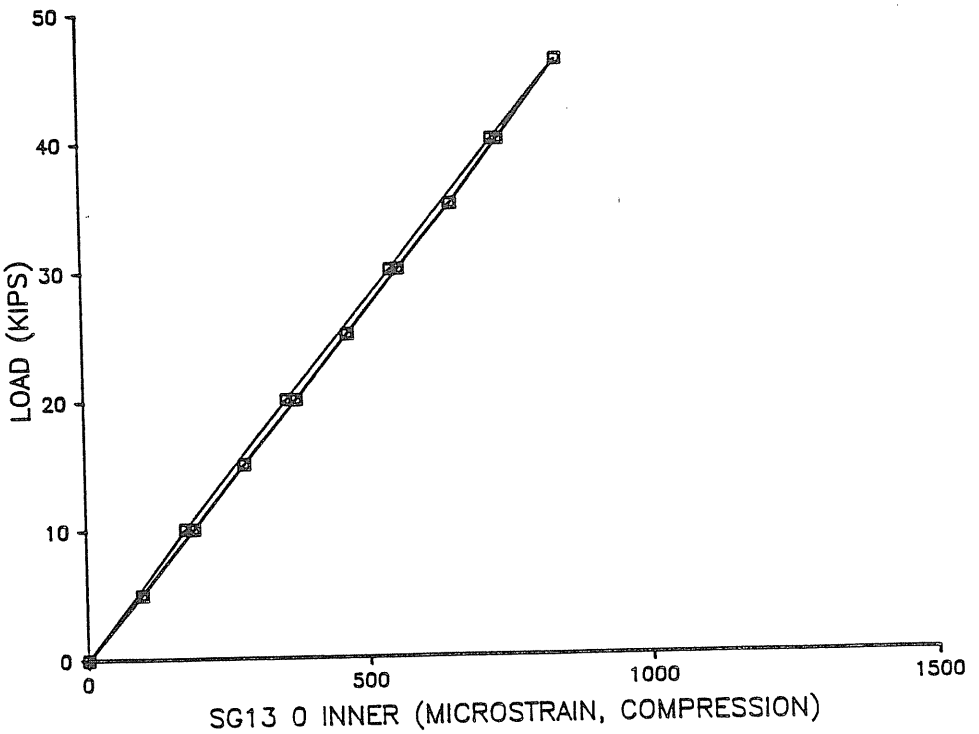

Figure B.43